

Distributed Detection for Centralized and Decentralized Millimeter Wave Massive MIMO Sensor Networks

Apoorva Chawla, *Student Member, IEEE*, Rakesh Kumar Singh, *Student Member, IEEE*, Adarsh Patel, *Member, IEEE*, Aditya K. Jagannatham, *Member, IEEE* and Lajos Hanzo, *Fellow, IEEE*

Abstract—Multi-sensor millimeter wave (mmWave) massive multiple-input multiple-output (MIMO) wireless sensor networks (WSNs) relying on both distributed (D-MIMO) and centralized (C-MIMO) configurations are conceived. Hybrid combining based low complexity fusion rules are constructed for the fusion center (FC) for both D-MIMO and C-MIMO systems employing a partially connected structure (PCS) and a fully connected structure (FCS), respectively. The decision rules are based on the transmission of local binary sensor decisions and also take into account the accuracy of local detection at the individual sensors. Closed-form analytical expressions are derived for the probabilities of false alarm and correct detection to analyze the system's performance. Furthermore, the asymptotic distributed detection (DD) performance corresponding to both antenna architectures is analyzed in the large-scale antenna regime along with the pertinent power scaling laws. Additionally, digital signaling matrices are designed for enhancing the system performance. Our simulation results quantify the performance gains of the proposed architectures, which closely match the analytical results.

Index Terms— Millimeter wave, distributed detection, massive multiple-input multiple-output, centralized, distributed, hybrid combining, Neyman-Pearson criterion, wireless sensor networks.

I. INTRODUCTION

NEXT GENERATION 5G systems are expected to integrate wireless sensor networks (WSNs) relying on ultra-dense sensor deployment for supporting the Internet of things (IoT) and mission critical applications related to disaster management, surveillance, health care, vehicular communication,

drones, and several others [2]. Millimeter-wave (mmWave) carrier frequencies ranging from 30 to 300 GHz are eminently suitable for meeting the growing throughput and connectivity demands of such large scale sensor networks [3]. However, the practical implementation of mmWave communication is significantly more challenging than communications in the sub-6 GHz bands because of the higher path losses and severe signal blockages [4]. The problem is further aggravated by the increased hardware complexity of sampling and processing such high-bandwidth signals.

However, the mmWave band is still deemed appropriate, because mmWave frequencies facilitate the deployment of large antenna arrays, since the substantially reduced wavelength enables close packing of a large number of antennas within limited physical dimensions, which in turn helps in compensating the increased propagation losses by the resultant high array gains. Thus, massive MIMO technology, wherein the base station (BS) is equipped with a very large antenna array comprising of hundreds of antennas [5], is an excellent candidate for overcoming the above impediments in the practical realization of mmWave communication. Additionally, massive MIMO technology has the attractive ability to enable simultaneous connectivity and communication with a large number of sensors using spatial multiplexing. Moreover, it allows for a significant transmit power reduction of the sensors [6], thereby extending the battery life of the sensors. Therefore, mmWave massive MIMO systems are well-suited for sensing and communication in ultra-dense sensor networks. A brief review of the existing literature is presented next.

A. Review of the Literature

Efficient processing of signals in mmWave massive MIMO systems is crucial for achieving the promised high data rates. However, the conventional fully digital signal processing architecture, wherein signal processing is performed exclusively in the baseband, necessitates a dedicated radio frequency (RF) chain for each antenna. Such a transceiver architecture is both costly and power-thirsty owing to the high power consumption of analog-to-digital converters (ADCs) at mmWave frequencies. To reduce the complexity, hybrid signal processing architectures, which process the signal in a mixture of analog and digital domains, have emerged as a popular choice for mmWave MIMO implementation [18], [19]. Thus, by minimizing the number of RF chains and

Copyright (c) 2015 IEEE. Personal use of this material is permitted. However, permission to use this material for any other purposes must be obtained from the IEEE by sending a request to pubs-permissions@ieee.org.

This work was presented in part at the 2020 Int. Conf. Signal Process. Commun. (SPCOM), Bangalore, India, July 2020 [1].

A. Chawla, R. K. Singh and A. K. Jagannatham are with the Department of Electrical Engineering, Indian Institute of Technology Kanpur, Kanpur, UP 208016, India (e-mail: {capoorva, singhrk, adityaj}@iitk.ac.in).

A. Patel is with the School of Computing and Electrical Engineering, Indian Institute of Technology Mandi, HP 175005, India (e-mail: adarsh@iitmandi.ac.in).

L. Hanzo is with the Department of Electronics and Computer Science, University of Southampton, Southampton SO17 1BJ, UK (e-mail: lh@ecs.soton.ac.uk). This work was supported in part by the Science and Engineering Research Board (SERB), Department of Science and Technology, Government of India, in part by the Space Technology Cell, IIT Kanpur, in part by the IIMA IDEA Telecom Centre of Excellence, in part by the Qualcomm Innovation Fellowship, and in part by the Arun Kumar Chair Professorship. L. Hanzo would like to acknowledge the financial support of the Engineering and Physical Sciences Research Council projects EP/P034284/1 and EP/P003990/1 (COALESCE) as well as of the European Research Council's Advanced Fellow Grant QuantCom (Grant No. 789028).

Table I
CONTRASTING OUR CONTRIBUTION TO THE LITERATURE

	[7]	[8]	[9]	[10]	[11]	[12]	[13]	[14]	[15]	[16]	[17]	Proposed Work
Distributed Detection							✓	✓	✓	✓	✓	✓
MIMO WSN							✓	✓	✓	✓	✓	✓
mmWave Communication		✓	✓	✓	✓							✓
Massive MIMO	✓	✓		✓		✓				✓	✓	✓
Hybrid combining		✓			✓							✓
C-MIMO Architecture	✓	✓	✓	✓	✓	✓	✓	✓	✓	✓	✓	✓
D-MIMO Architecture	✓	✓	✓	✓	✓	✓						✓
Large array analysis	✓					✓				✓	✓	✓
Simplified test statistic								✓	✓	✓	✓	✓
Large-scale fading	✓	✓		✓		✓				✓	✓	✓
Power scaling analysis	✓					✓				✓	✓	✓
Signaling optimization											✓	✓
Practical BS/ FC selection algorithm		✓										✓

hence the power consumption, without significantly impacting the spectral efficiency (SE), these transceiver designs have significantly eased the practical realization of mmWave MIMO systems. Low complexity hybrid analog-digital transmit and receive beamforming/ equalizing techniques are proposed in [11] for the uplink (UL) of mmWave massive MIMO HetNets to alleviate the inter- and intra-tier interferences. Li *et al.* [20] proposed a low complexity hybrid beamforming algorithm for multiuser (MU) mmWave MIMO systems to reduce the inter-user interference arising due to diffused scattering. Furthermore, Chen *et al.* [21] designed a hybrid transmit precoding algorithm to cancel successive interference for generalized subarray-connected architectures considering arbitrary RF chain and antenna configurations to maximize the total achievable rate. A distance-dependent beamforming gain based hybrid beamformer is designed in [22] for MU mmWave systems, where the RF chains are grouped together to serve a particular cluster of users depending on the channel conditions. Cai *et al.* [23] maximized the worst-case sum rate by jointly optimizing the hybrid beamforming matrices at the relay stations and the BS using the penalty dual decomposition method for MU mmWave full-duplex MIMO relay systems.

Although, the implementation of the centralized antenna architecture (C-MIMO) has a lower cost and complexity, the close packing of a large number of antennas together with the sparse nature of the multi-path wireless channel at the mmWave frequencies leads to a high degree of spatial channel correlation, which can in turn lead to poor performance in the C-MIMO systems. An attractive technique of reducing the channel correlation in such systems is to use distributed MIMO (D-MIMO) configurations, where a massive antenna array is distributed over dispersed geographical locations. Employing the distributed antenna architecture helps to mitigate the channel correlation, reduce the radio access distance and enhance the system performance. Interestingly, D-MIMO systems have also been shown to improve the coverage quality in indoor wireless networks [24]–[26]. Furthermore, the distributed architecture facilitates significant power and SE gains over its centralized counterpart due to the reduced propagation distance between the sensors and the BS [27]–[30]. The UL SE of D-MIMO systems considering zero forcing (ZF) receivers is examined and compared to that of C-MIMO systems in

[12], along with its analysis in the large-scale antenna regime. The framework is further extended to a multicell D-MIMO scenario, while also factoring in the impact of cochannel interference. The SE of a hybrid precoding/ combining based downlink (DL) MU mmWave massive MIMO system was analyzed in [8] considering both centralized and distributed architectures. Gimenez *et al.* [9] proposed a distributed hybrid precoding algorithm and analyzed the performance of an indoor mmWave D-MIMO system. The treatise in [31] exhaustively reviews the developments in symbol detection for space division multiplexing (SDM)-based MIMO systems considering various techniques such as linear MIMO detectors, interference cancellation aided MIMO detectors, tree-search based MIMO detectors, lattice-reduction aided detectors etc. Yue and Nguyen [10] analyzed the multiplexing gain of a mmWave massive MIMO system relying on a distributed subarray architecture, when the number of antennas at the subarrays grows large and the transmit power is kept constant. Typically three dominant hardware architectures are considered for implementation of hybrid signal processing in mmWave massive MIMO systems, namely the fully connected structure (FCS) [32], hybridly connected structure (HCS) [33] and partially-connected structure (PCS) [34], [35]. Several authors have shown [8], [34] that systems incorporating PCS consume lower power as a benefit of its lower implementation complexity in comparison to their FCS and HCS-based counterparts. Explicitly, the former requires a much lower number of phase shifters. Thus, due to its compelling advantages, the PCS-based D-MIMO architecture is also considered in this study in addition to the conventional C-MIMO configuration.

There are quiet a few contributions on attractive distributed detection (DD) schemes [13]–[17], [36], [37]. Li and Dai [36] presented a multiple access (MAC) framework for DD in a WSN having correlated sensor observations. Banavar *et al.* [14] investigated a fading MAC DD scenario, where the sensors employ amplify-and-forward relaying for transmitting their observations to a FC equipped with multiple antennas. Furthermore, Ciuonzo *et al.* [15] proposed sub-optimal fusion rules utilizing the decode-then-fuse as well as decode-and-fuse principles for a MIMO channel. Authors in [38] developed Neyman-Pearson (NP) and generalized likelihood ratio test (GLRT)-based detectors at the fusion center (FC)

for known and unknown parameter detection. Jiang *et al.* [39] investigated the estimation and detection performance of a coherent amplify-and-forward massive MIMO WSN using the linear minimum mean-squared error estimator (LMMSE), NP and energy detectors. The large number of 5G IoT applications requires dense sensor deployment, which in turn necessitates substantial time-bandwidth resources to support data transmission from the large number of sensors in each unit area. Needless to say, since 5G has to support thousands of sensors [40], the transmission of raw measurements from a large sensor sprawl to the FC may lead to congestion in next generation wireless networks. Therefore, due to practical power and bandwidth constraints, it is prudent to compress the sensor measurements locally prior to transmission to the FC. This can then be followed by efficient processing of the local decisions at the FC to form a final decision with respect to the signal/ phenomenon of interest [41]–[43]. Moreover, the performance of MIMO sensor networks can be significantly enhanced by the presence of a massive antenna array at the FC. The performance benefits of using a massive antenna array at the FC for DD has been analyzed in [13], [16], [17], [37]. A collection of low-complexity decision rules have been formulated in [16] for DD in massive MIMO systems. Chawla *et al.* [37] have derived linear filtering based low-complexity fusion rules for massive MIMO WSNs using antipodal signaling, while also considering the reliabilities of the local sensor decisions. This framework was then further extended to the non-antipodal signaling format in [17], followed by its asymptotic performance analysis relying on both perfect and imperfect CSI. Jarrah *et al.* derived fusion rules for a decode-and-forward relaying based cooperative WSN in [13]. The authors of [44] proposed energy detection-based rules for decision fusion in WSNs. The analysis therein considers a Gaussian mixture channel model between the sensors and the FC for a non-massive MIMO system and specific results are presented for *Rice*, *2ZM* and *NZZ fading*. However, due to the absence of a massive antenna array, the framework of [44] is unable to leverage the gains arising from a large number of antennas at the FC. Moreover, the schemes proposed in [44] are based on energy detection, which has suboptimal performance in comparison to the coherent detector.

However, none of the existing treatises have utilized hybrid combining at the FC for exploiting the advantages of mmWave massive MIMO technology for DD, hence their fusion rules are unknown. To fill this knowledge-gap, we analyse a mmWave massive MIMO system, where hybrid combining based low-complexity fusion rules are conceived for detecting the absence/ presence of a signal of interest. In the early conference version of this paper [1], a decision rule based on hybrid combining was used for the C-MIMO architecture. This paper extends the framework to a distributed MIMO topology along with its performance analysis in terms of the closed-form analytical expressions derived for the probabilities of correct detection and false alarm. Furthermore, an efficient transmit signaling matrix is designed for the D-MIMO system. Additionally, the asymptotic DD performance is analyzed in the large-scale antenna regime for both D-MIMO and C-MIMO scenarios, which is lacking in [1]. The

main contributions of this paper are summarized below, which are boldly and explicitly contrasted to the relevant literature in Table I.

B. Our Contributions

- This paper investigates a multiple-observation based vector model for DD, wherein each sensor transmits a binary decision vector over one or more signaling intervals corresponding to its local decision, which is prone to errors. This is different from the systems in [14], [45], [46] that consider the transmission of analog sensor observations.
- A low-complexity detection rule based on centralized hybrid combining, leveraging the antenna array response vectors, is derived for the centralized (C-MIMO) architecture, in contrast to [14], [38], [45] that focus on DD with analog observations. The mmWave WSN framework is further extended to a distributed antenna architecture, where the antenna array is split among multiple spatially separated FCs located on a circle. To reduce the radio access distance and improve the system performance, a minimum distance based (D-selection) method is utilized for assigning each sensor to a FC. Furthermore, a distributed hybrid combining-based detection rule, which employs distributed RF combining followed by centralized baseband combining, is conceived for a D-MIMO WSN relying on the D-selection scheme. Explicitly, we go beyond the scope of [15]–[17] which derive fusion rules only for a centralized massive MIMO WSN.
- Analytical results are derived for characterizing the system performance in terms of the probabilities of correct detection P_D and false alarm P_{FA} at the FC for both antenna configurations. Furthermore, the transmit signaling matrices are determined for both the C- and D-MIMO sensor networks that achieve a significant performance gain.
- The pertinent power-scaling laws are also determined in the large-scale antenna regime based on closed-form asymptotic expressions. It is explicitly demonstrated that each sensor can reduce its transmit power in proportion to $1/M$ and $1/N_f$ for the centralized and distributed schemes, respectively, without degrading its performance. This in turn results in prolonged battery life for the sensors, ensuring reliable WSN operation. This is in contrast to [16], [17] that characterize the asymptotic performance only for centralized massive MIMO systems.

The rest of the paper is organized as follows. Section II describes the system model of both C- and D-MIMO based WSNs. Furthermore, hybrid combining based fusion rules and the probabilities of false alarm and correct detection are derived in Section III for both the above antenna configurations. Section IV presents our large-scale antenna array analysis, followed by the associated signaling matrix design in Section V. Our probability of error expressions are derived in Section VI, while Section VII describes our exhaustive simulation study. Our conclusions are drawn in Section VIII.

The following notation is used throughout the paper: Boldface uppercase letters \mathbf{Y} and boldface lowercase letters \mathbf{y}

are utilized to represent matrices and vectors, respectively, where $[\mathbf{Y}]_{i,j}$ and y_i denote their respective (i, j) th and i th entries. The letters $\mathbf{Y}^{(i)}$ and $\mathbf{y}^{(i)}$ are used to represent the matrix and the vector obtained during the i th iteration. $\Pr(C|D)$ and $\Pr(\cdot)$ indicate the conditional probability of event C given D and the probability of an event, respectively. Further, $p(\cdot)$ denotes the probability density function (PDF). The Gaussian Q-function, represented by Q , is expressed as $Q(x) = \frac{1}{\sqrt{2\pi}} \int_x^\infty \exp(-\frac{m^2}{2}) dm$. The matrix \mathbf{I}_L indicates an $L \times L$ identity matrix. The notation $\mathcal{CN}(\boldsymbol{\mu}, \mathbf{C})$ is used to represent the complex Gaussian distribution with mean $\boldsymbol{\mu}$ and covariance matrix \mathbf{C} . The mathematical operators little-o, real part, expectation operator, absolute value, conjugate and exponential operator are represented by $o(\cdot)$, $\Re\{\cdot\}$, $\mathbb{E}\{\cdot\}$, $|\cdot|$, $(\cdot)^*$ and $\exp(\cdot)$, respectively. Furthermore, the operators conjugate transpose, Euclidean norm, inverse vec operator, transpose, weighted norm and vec operator are denoted by $(\cdot)^H$, $\|\cdot\|$, $\text{vec}^{-1}(\cdot)$, $(\cdot)^T$, $\|\cdot\|_{\mathbf{X}}$ and $\text{vec}(\cdot)$, respectively.

II. SYSTEM MODEL

Consider a distributed mmWave massive MIMO sensor network, where multiple sensors observe a specific signal of interest to differentiate between the binary hypotheses of the set $\mathcal{H} = \{\mathcal{H}_0, \mathcal{H}_1\}$. In this binary hypothesis testing problem, the alternative hypothesis \mathcal{H}_1 and the null hypothesis \mathcal{H}_0 correspond to the presence and absence of the signal of interest, respectively. The k th sensor, $1 \leq k \leq K$, makes a local binary decision regarding the observed signal of interest. Subsequently, it transmits this local decision by modulating it as the signal vector $\mathbf{x}_k = [x_k(1), x_k(2), \dots, x_k(N)]^T \in \mathbb{C}^{N \times 1}$. The symbols $x_k(i)$ are transmitted over N signaling intervals on the basis of the local binary decision. For instance, for the standard antipodal signaling scheme, the transmitted local binary decision vectors can belong to the set $\mathbf{x}_k \in \{\mathbf{u}_k, -\mathbf{u}_k\}$, where \mathbf{u}_k and $-\mathbf{u}_k$ encode the presence or absence of the signal of interest, respectively. The local probabilities of false alarm $P_{F,k}$ and correct detection $P_{D,k}$ of the k th sensor are defined as

$$\begin{aligned} P_{F,k} &= \Pr(\mathbf{x}_k = \mathbf{u}_k | \mathcal{H}_0), \\ P_{D,k} &= \Pr(\mathbf{x}_k = \mathbf{u}_k | \mathcal{H}_1). \end{aligned} \quad (1)$$

In a mmWave massive MIMO based WSN, K single-antenna sensors are employed, wherein the sensors simultaneously communicate with the FC over a flat-fading coherent MAC whose carrier frequency is in the mmWave band. The terminologies of sensors and FC are widely used in the existing literature on distributed detection [1], [13]–[17], [36]–[38], [41]–[43], [45]–[47]. The FC can employ different antenna architectures, namely the centralized and distributed MIMO configurations, denoted by C-MIMO and D-MIMO, respectively. The C-MIMO employs FCS, where each RF chain is connected to all the FC antennas, whereas the D-MIMO utilizes PCS, where only a single RF chain can access the antenna sub-array at each FC. In the C-MIMO WSN, all the K sensors are associated with a single FC deployed at the cell center, whereas in the D-MIMO WSN, one sensor is assigned to a single FC based on the minimum distance criterion. Finally, the C-MIMO WSN employs a centralized

RF and baseband combining at the FC located at the cell center, whereas in the D-MIMO WSN, the RF combining is carried out individually at each FC, followed by a centralized baseband combining of the RF combiner outputs from K FCs at the baseband processing unit (BPU). Both the architectures are described in detail in the following subsections.

A. C-MIMO Based FC

In the C-MIMO system based on FCS, the FC located at the cell center is equipped with a massive co-located antenna array comprised of M antennas, such that $M \gg K$, as illustrated in Fig. 1a. Additionally, the total number of RF chains N_{RF} is assumed to be $N_{RF} = K$, which implies that the FC uses only a single data stream to communicate with each sensor. The signal $\mathbf{y}(n) \in \mathbb{C}^{M \times 1}$ received at the FC during the n th, $1 \leq n \leq N$, signaling interval can be expressed as

$$\mathbf{y}(n) = \sqrt{p_u} \mathbf{G} \mathbf{x}(n) + \mathbf{w}(n), \quad (2)$$

where p_u is the average transmit power of each sensor, $\mathbf{x}(n) = [x_1(n), x_2(n), \dots, x_K(n)]^T \in \mathbb{C}^{K \times 1}$ is the transmit signal vector obtained by concatenating the symbols of all the K sensors during the n th signaling interval and $\mathbf{w}(n) \in \mathbb{C}^{M \times 1}$ denotes the additive white Gaussian noise (AWGN) vector distributed as $\mathcal{CN}(0, \sigma_w^2 \mathbf{I}_M)$. The matrix $\mathbf{G} = [\mathbf{g}_1, \mathbf{g}_2, \dots, \mathbf{g}_K] \in \mathbb{C}^{M \times K}$ represents the mmWave channel between the K sensors and the FC for the centralized antenna configuration. The channel vector $\mathbf{g}_k \in \mathbb{C}^{M \times 1}$ between the FC and the k th sensor can be formulated as $\mathbf{g}_k = \sqrt{\beta_k} \mathbf{h}_k$, where the large-scale fading coefficient β_k between the FC and the k th sensor accounts for the log-normal shadowing and pathloss effects that are assumed to be constant across m , $1 \leq m \leq M$. Adopting the narrowband channel model based on the extended Saleh-Valenzuela model, which accurately captures the characteristics of mmWave channels [48], the small-scale fading vector $\mathbf{h}_k \in \mathbb{C}^{M \times 1}$ between the k th sensor and the FC can be modeled as

$$\mathbf{h}_k = \sqrt{\frac{M}{L_k}} \sum_{l=1}^{L_k} \alpha_k^l \mathbf{a}_r(\theta_k^l), \quad (3)$$

where $\alpha_k^l \sim \mathcal{CN}(0, 1)$ denotes the complex gain of the l th path. The quantity L_k is the number of propagation paths for the channel of the k th sensor and follows the discrete uniform distribution $L_k \sim \mathcal{DU}[1, L_m]$, where L_m represents the maximum number of propagation paths, which is known at the FC. The angle θ_k^l represents the angle of arrival (AoA) of the l th multipath from the k th sensor, which is assumed to be uniformly distributed in the interval $[0, 2\pi]$. Considering a standard uniform linear array (ULA) at the FC, the receive array response vector corresponding to the AoA θ_k^l , denoted by $\mathbf{a}_r(\theta_k^l) \in \mathbb{C}^{M \times 1}$, is expressed as

$$\mathbf{a}_r(\theta_k^l) = \frac{1}{\sqrt{M}} \left[1, e^{jv \sin(\theta_k^l)}, \dots, e^{jv(M-1) \sin(\theta_k^l)} \right]^T, \quad (4)$$

where $v = \frac{2\pi}{\lambda} d$, λ is the carrier wavelength and d is the inter-element spacing. Hence, the resultant channel matrix \mathbf{G} can be modeled as $\mathbf{G} = \mathbf{H} \mathbf{D}^{1/2}$, where \mathbf{D} is the large-scale fading diagonal matrix with β_k , $1 \leq k \leq K$, along

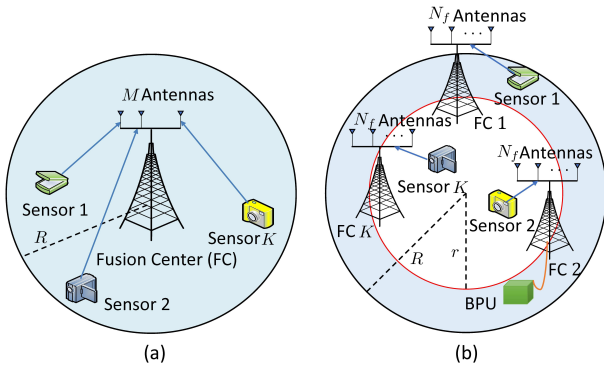


Figure 1. MmWave massive MIMO WSN antenna architectures (a) Centralized (b) Distributed with circular layout.

its principal diagonal and $\mathbf{H} = [\mathbf{h}_1, \mathbf{h}_2, \dots, \mathbf{h}_K] \in \mathbb{C}^{M \times K}$ is the small-scale fading matrix. Using (2), the composite signal $\mathbf{Y} \in \mathbb{C}^{M \times N}$ received at the FC corresponding to the transmissions of all the sensors can be expressed as

$$\mathbf{Y} = \sqrt{p_u} \mathbf{G} \mathbf{X} + \mathbf{W}, \quad (5)$$

where $\mathbf{W} = [\mathbf{w}(1), \dots, \mathbf{w}(N)] \in \mathbb{C}^{M \times N}$ is the noise matrix obtained via concatenation of the N AWGN vectors $\mathbf{w}(n)$, so that its elements $w_{s,t}(n)$ are independent and identically distributed (i.i.d.) and obey the distribution $w_{s,t}(n) \sim \mathcal{CN}(0, \sigma_w^2)$ and $\mathbf{X} \in \mathbb{C}^{K \times N}$ is the transmitted signal matrix.

B. D-MIMO Based FC

In a distributed mmWave massive MIMO WSN, multiple FCs with separate antenna arrays are spatially separated and are connected together by a high capacity backhaul, such as a fiber optic link, as demonstrated in Fig. 1b. This employs the PCS, where only a single RF chain is connected to the antenna sub array at each FC through an RF combiner. Furthermore, the RF combiner outputs of all the FCs are fed to a central BPU. A total of J FCs, each equipped with an antenna array comprised of N_f antennas, communicate with K single-antenna sensors. Under the assumption that $J = K$, i.e. the total number of sensors is restricted to the number of FCs, the total number of antennas at all the FCs is $N_{tot} = KN_f$. It should be noted that in order to make a fair comparison, the total number of RF chains N_{RF} as well as the total number of antennas at the FC N_{tot} are kept identical to that of the centralized system, i.e., $N_{RF} = K$ and $N_{tot} = M$. For this scenario, the signal $\mathbf{y}_j(n) \in \mathbb{C}^{N_f \times 1}$, $1 \leq j \leq K$, received at the j th FC during the n th signaling instant corresponding to the transmitted signal vector $\mathbf{x}(n)$, can be represented as

$$\mathbf{y}_j(n) = \sqrt{p_u} \mathbf{G}_j \mathbf{x}(n) + \mathbf{w}_j(n), \quad (6)$$

where $\mathbf{w}_j(n) \in \mathbb{C}^{N_f \times 1}$ is the AWGN vector at the j th FC with its elements obeying $w_{f,j}(n) \sim \mathcal{CN}(0, \sigma_w^2)$, $1 \leq f \leq N_f$ and $\mathbf{G}_j = [\mathbf{g}_{1,j}, \mathbf{g}_{2,j}, \dots, \mathbf{g}_{K,j}] \in \mathbb{C}^{N_f \times K}$ is the composite mmWave channel between the K sensors and the j th FC. Considering N signaling instants, the signal $\mathbf{Y}_j \in \mathbb{C}^{N_f \times N}$ received at the j th FC, $1 \leq j \leq K$, can be expressed as

$$\mathbf{Y}_j = \sqrt{p_u} \mathbf{G}_j \mathbf{X} + \mathbf{W}_j, \quad (7)$$

where $\mathbf{W}_j = [\mathbf{w}_j(1), \dots, \mathbf{w}_j(N)] \in \mathbb{C}^{N_f \times N}$ denotes the receiver noise matrix at the j th FC with its elements $w_{s,t,j}(n)$ distributed as $w_{s,t,j}(n) \sim \mathcal{CN}(0, \sigma_w^2)$. Similar to the C-MIMO system, the channel vector $\mathbf{g}_{k,j} \in \mathbb{C}^{N_f \times 1}$ between the j th FC and the k th sensor can be expressed as $\mathbf{g}_{k,j} = \sqrt{\beta_{k,j}} \mathbf{h}_{k,j}$, where $\beta_{k,j}$ and $\mathbf{h}_{k,j}$ denote the large-scale fading coefficient and the small-scale fading vector between the j th FC and the k th sensor. Using the narrowband channel model, the small-scale fading vector $\mathbf{h}_{k,j}$ can be characterized as

$$\mathbf{h}_{k,j} = \sqrt{\frac{N_f}{L_{k,j}}} \sum_{l=1}^{L_{k,j}} \alpha_{k,j}^l \mathbf{a}_r(\theta_{k,j}^l), \quad (8)$$

where $\theta_{k,j}^l \in [0, 2\pi]$ and $\alpha_{k,j}^l \sim \mathcal{CN}(0, 1)$ represent the AoA and the complex gain corresponding to the k th sensor, l th path and the j th FC, respectively. The parameter $L_{k,j}$ indicates the number of propagation paths between the j th FC and the k th sensor that is distributed as a discrete uniform random variable in the interval $[1, L_m]$, where L_m is the maximum number of propagation paths. The receive array response vector $\mathbf{a}_r(\theta_{k,j}^l) \in \mathbb{C}^{N_f \times 1}$ at the j th FC corresponding to the k th sensor can be modeled as

$$\mathbf{a}_r(\theta_{k,j}^l) = \frac{1}{\sqrt{N_f}} \left[1, e^{jv \sin(\theta_{k,j}^l)}, \dots, e^{jv(N_f-1) \sin(\theta_{k,j}^l)} \right]^T.$$

Hence, the resultant mmWave massive MIMO channel matrix \mathbf{G}_j corresponding to the j th FC can be expressed as

$$\mathbf{G}_j = \mathbf{H}_j \mathbf{D}_j^{1/2}, \quad (9)$$

where $\mathbf{H}_j = [\mathbf{h}_{1,j}, \mathbf{h}_{2,j}, \dots, \mathbf{h}_{K,j}] \in \mathbb{C}^{N_f \times K}$ represents the small-scale fading matrix obtained using (8) and \mathbf{D}_j is the large-scale fading matrix with the principal diagonal elements of $\beta_{k,j}$, $1 \leq k \leq K$, for the j th FC. Utilizing the above framework, our fusion rules are derived next for the mmWave massive MIMO WSN, under different antenna configurations.

III. FUSION RULE WITH HYBRID COMBINING

This section develops the fusion rules for the FC considering both centralized and distributed antenna configurations.

A. Fusion Rule for C-MIMO Based WSN

Utilizing the NP criterion [49], which aims for maximizing the probability of correct detection for a given probability of false alarm, the log likelihood ratio (LLR) test for the received signal \mathbf{Y} in (5), considering a centralized antenna topology can be formulated as

$$T(\mathbf{Y}) = \ln \left[\frac{p(\mathbf{Y}|\mathcal{H}_1)}{p(\mathbf{Y}|\mathcal{H}_0)} \right] \underset{\mathcal{H}_0}{\overset{\mathcal{H}_1}{\gtrless}} \gamma, \quad (10)$$

where $p(\mathbf{Y}|\mathcal{H}_0)$, $p(\mathbf{Y}|\mathcal{H}_1)$ are the PDFs of the observation matrix \mathbf{Y} under the hypotheses of \mathcal{H}_0 and \mathcal{H}_1 , respectively and γ denotes the detection threshold. The LLR test in (10) evaluates the sum of $p[\mathbf{y}(n)|\mathbf{x}(n)]\Pr[\mathbf{x}(n)|\mathcal{H}_i]$, where $i = \{0, 1\}$, over 2^K combinations of the transmit vector $\mathbf{x}(n)$, which can be simplified to obtain

$$T(\mathbf{Y}) = \sum_{n=1}^N \ln \left[\frac{\sum_{\mathbf{x}(n)} p(\mathbf{y}(n)|\mathbf{x}(n)) \Pr(\mathbf{x}(n)|\mathcal{H}_1)}{\sum_{\mathbf{x}(n)} p(\mathbf{y}(n)|\mathbf{x}(n)) \Pr(\mathbf{x}(n)|\mathcal{H}_0)} \right] \quad (11)$$

$$= \sum_{n=1}^N \ln \left[\frac{\sum_{\mathbf{x}(n)} \exp\left(-\frac{\|\mathbf{y}(n) - \sqrt{p_u} \mathbf{G} \mathbf{x}(n)\|^2}{\sigma_w^2}\right) \Pr(\mathbf{x}(n)|\mathcal{H}_1)}{\sum_{\mathbf{x}(n)} \exp\left(-\frac{\|\mathbf{y}(n) - \sqrt{p_u} \mathbf{G} \mathbf{x}(n)\|^2}{\sigma_w^2}\right) \Pr(\mathbf{x}(n)|\mathcal{H}_0)} \right], \quad (12)$$

where the expression in (11) follows from the independence of the transmitted signal vectors $\mathbf{x}(n)$ across the N signaling intervals and (12) is arrived at by substituting the PDF $p(\mathbf{y}(n)|\mathbf{x}(n))$, that is given as

$$p(\mathbf{y}(n)|\mathbf{x}(n)) = \frac{1}{(\pi\sigma_w^2)^M} \exp\left[-\frac{1}{\sigma_w^2} \|\mathbf{y}(n) - \sqrt{p_u} \mathbf{G} \mathbf{x}(n)\|^2\right].$$

To reduce the complexity of its practical implementation, the LLR test $T(\mathbf{Y})$ is approximated by the two-step solution outlined below. In the first step, the observation matrix \mathbf{Y} is processed using a hybrid combiner, which is the combination of an analog combiner $\mathbf{F}_{\text{RF}} \in \mathbb{C}^{M \times K}$ and a digital combiner $\mathbf{F}_{\text{BB}} \in \mathbb{C}^{K \times K}$, to obtain the soft decisions of the sensors, as shown in Fig. 2. It should be noted that the number of RF chains required for hybrid combining is $N_{\text{RF}} = K$, which is much lower in comparison to fully digital combining, which requires one RF chain per antenna, i.e. a total of M RF chains at the FC, where $M \gg K$. The output matrix $\mathbf{Z} = [\mathbf{z}(1), \dots, \mathbf{z}(N)] \in \mathbb{C}^{K \times N}$, obtained from the hybrid combiner, can be expressed as

$$\mathbf{Z} = \mathbf{F}_{\text{BB}}^H \mathbf{F}_{\text{RF}}^H \mathbf{Y} = \sqrt{p_u} \mathbf{F}_{\text{BB}}^H \mathbf{F}_{\text{RF}}^H \mathbf{G} \mathbf{X} + \mathbf{F}_{\text{BB}}^H \mathbf{F}_{\text{RF}}^H \mathbf{W}. \quad (13)$$

Similar to [19], the analog combiner \mathbf{F}_{RF} of mmWave massive MIMO systems is constructed by stacking the optimal combining vectors equal to the receive array response vectors corresponding to their maximum path gains of the individual sensors, which has the structure of

$$\mathbf{F}_{\text{RF}} = [\mathbf{a}_r(\theta_1^{l_1}), \dots, \mathbf{a}_r(\theta_K^{l_K})], \quad (14)$$

where l_k is the path of the k th sensor with the maximum gain $|\alpha_k^{l_k}|$ and $\theta_k^{l_k}$, $1 \leq k \leq K$, denotes the corresponding AoA. The digital combiner \mathbf{F}_{BB} derived using the equivalent baseband channel matrix can be expressed as $\mathbf{F}_{\text{BB}} = \mathbf{F}_{\text{RF}}^H \mathbf{G}$. Invoking the asymptotic orthogonality property of mmWave massive MIMO channels [50] leads to

$$\mathbf{a}_r^H(\theta_k^{l_u}) \mathbf{a}_r(\theta_s^{l_v}) = \begin{cases} 1, & u = v \text{ and } k = s \\ 0, & u \neq v \text{ or } k \neq s \end{cases}, \quad (15)$$

as M tends to infinity and $L_k \ll M$, i.e. $L_k = o(M)$, $\forall k$. Thus, we can employ a diagonal baseband combiner \mathbf{F}_{BB} with its k th diagonal element set as $[\mathbf{F}_{\text{BB}}]_{k,k} = \sqrt{\frac{M\beta_k}{L_k}} \alpha_k^{l_k}$. Substituting the above choice of \mathbf{F}_{RF} and \mathbf{F}_{BB} in (13) and using the result derived in (15), the hybrid combiner output vector $\mathbf{z}_k \in \mathbb{C}^{N \times 1}$, of the k th sensor, can be derived as

$$\mathbf{z}_k = \sqrt{p_u} \frac{M\beta_k}{L_k} \left| \alpha_k^{l_k} \right|^2 \mathbf{x}_k + \tilde{\mathbf{w}}_k, \quad (16)$$

where $\tilde{\mathbf{w}}_k = \sqrt{\frac{M\beta_k}{L_k}} (\alpha_k^{l_k})^* (\mathbf{a}_r^H(\theta_k^{l_k}) \mathbf{W})^T \in \mathbb{C}^{N \times 1}$ is the equivalent AWGN vector that is distributed as $\tilde{\mathbf{w}}_k \sim \mathcal{CN}(\mathbf{0}, \mathbf{C}_{\tilde{\mathbf{w}}_k})$. The covariance matrix $\mathbf{C}_{\tilde{\mathbf{w}}_k} \in \mathbb{C}^{N \times N}$ and the constant d_k are defined as $\mathbf{C}_{\tilde{\mathbf{w}}_k} = M\sigma_w^2 d_k \mathbf{I}_N$ and

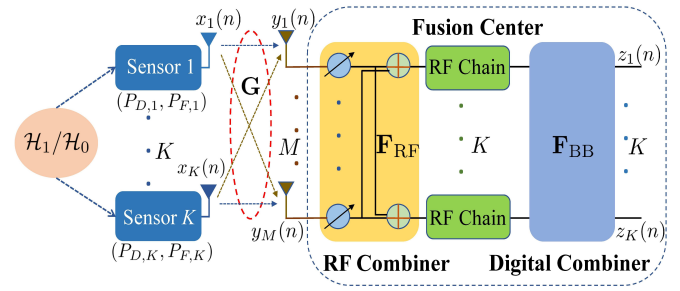


Figure 2. System model for distributed detection in a centralized configuration based mmWave massive MIMO WSN.

$d_k \triangleq \frac{\beta_k}{L_k} \mathbb{E}\{|\alpha_k^{l_k}|^2\}$, respectively. Using (16), the distribution of the output vector \mathbf{z}_k can be determined as $\mathbf{z}_k \sim \mathcal{CN}(\sqrt{p_u} M d_k \mathbf{x}_k, \mathbf{C}'_k)$, where the covariance matrix obeys $\mathbf{C}'_k = \frac{p_u M^2 \beta_k^2}{L_k^2} \mathbf{x}_k \mathbf{x}_k^H \text{var}\{|\alpha_k^{l_k}|^2\} + \mathbf{C}_{\tilde{\mathbf{w}}_k}$. Leveraging the independence of the output vectors across different sensors, the LLR based test statistic $T_C(\mathbf{Z})$ for DD can be formulated as

$$T_C(\mathbf{Z}) = \ln \left[\frac{p(\mathbf{Z}|\mathcal{H}_1)}{p(\mathbf{Z}|\mathcal{H}_0)} \right] = \ln \left[\prod_{k=1}^K \frac{p(\mathbf{z}_k|\mathcal{H}_1)}{p(\mathbf{z}_k|\mathcal{H}_0)} \right], \quad (17)$$

where $p(\mathbf{z}_k|\mathcal{H}_1)$ and $p(\mathbf{z}_k|\mathcal{H}_0)$ are the PDFs of the hybrid combiner output vector \mathbf{z}_k under the hypotheses \mathcal{H}_1 and \mathcal{H}_0 , respectively. For the antipodal signaling scheme having transmit signal vectors of \mathbf{u}_k and $-\mathbf{u}_k$ representing the presence and absence of the signal of interest, respectively, the test statistic above can be simplified as shown in (18). Upon substituting the PDFs $p(\mathbf{z}_k|\mathbf{x}_k)$ for $\mathbf{x}_k \in \{\mathbf{u}_k, -\mathbf{u}_k\}$, determined in (19) and (20), respectively, with the covariance matrix $\tilde{\mathbf{C}}_k = \frac{p_u M^2 \beta_k^2}{L_k^2} \mathbf{u}_k \mathbf{u}_k^H \text{var}\{|\alpha_k^{l_k}|^2\} + \mathbf{C}_{\tilde{\mathbf{w}}_k} = M \mathbf{C}_k$, where the matrix \mathbf{C}_k is defined as $\mathbf{C}_k = \frac{p_u M \beta_k^2}{L_k^2} \mathbf{u}_k \mathbf{u}_k^H \text{var}\{|\alpha_k^{l_k}|^2\} + \sigma_w^2 d_k \mathbf{I}_N$ and the local sensor performance metrics from (1), the test statistic in (18) reduces to the expression below

$$T_C(\mathbf{Z}) = \sum_{k=1}^K \ln \left[\frac{P_{D,k} + (1 - P_{D,k}) \exp(-4\sqrt{p_u} d_k \Re(\mathbf{z}_k^H \mathbf{C}_k^{-1} \mathbf{u}_k))}{P_{F,k} + (1 - P_{F,k}) \exp(-4\sqrt{p_u} d_k \Re(\mathbf{z}_k^H \mathbf{C}_k^{-1} \mathbf{u}_k))} \right]. \quad (18)$$

The detailed derivation of the above expression is given in the technical report [51]. At low SNRs¹, using the approximations $\ln(1+x) \approx x$ and $e^{-x} \approx (1-x)$, the test statistic is further reduced to the compact form of

$$T_C(\mathbf{Z}) = \sum_{k=1}^K a_k d_k \Re(\mathbf{z}_k^H \mathbf{C}_k^{-1} \mathbf{u}_k) \underset{\mathcal{H}_0}{\overset{\mathcal{H}_1}{\gtrless}} \gamma', \quad (19)$$

where we have $a_k \triangleq P_{D,k} - P_{F,k}$, for the k th sensor. It is readily seen that the fusion rule obtained in (22) has a significantly reduced complexity as a benefit of its efficient linear combiner structure. For the special case of sensors relying on identical local performance metrics, i.e., $P_{D,k} = P_D$,

¹The low SNR regime is frequently encountered in sensor networks, as the sensor nodes typically operate at a very low transmit power levels due to battery constraints [42], [47]. Additionally, this minimizes the probability of unauthorized detection/ interception [41].

$$T_C(\mathbf{Z}) = \sum_{k=1}^K \ln \left[\frac{p(\mathbf{z}_k | \mathbf{x}_k = \mathbf{u}_k) \Pr(\mathbf{x}_k = \mathbf{u}_k | \mathcal{H}_1) + p(\mathbf{z}_k | \mathbf{x}_k = -\mathbf{u}_k) \Pr(\mathbf{x}_k = -\mathbf{u}_k | \mathcal{H}_1)}{p(\mathbf{z}_k | \mathbf{x}_k = \mathbf{u}_k) \Pr(\mathbf{x}_k = \mathbf{u}_k | \mathcal{H}_0) + p(\mathbf{z}_k | \mathbf{x}_k = -\mathbf{u}_k) \Pr(\mathbf{x}_k = -\mathbf{u}_k | \mathcal{H}_0)} \right] \quad (18)$$

$$p(\mathbf{z}_k | \mathbf{x}_k = \mathbf{u}_k) = \frac{1}{|\pi \tilde{\mathbf{C}}_k|} \exp \left(-(\mathbf{z}_k - \sqrt{p_u} M d_k \mathbf{u}_k)^H \tilde{\mathbf{C}}_k^{-1} (\mathbf{z}_k - \sqrt{p_u} M d_k \mathbf{u}_k) \right) \quad (19)$$

$$p(\mathbf{z}_k | \mathbf{x}_k = -\mathbf{u}_k) = \frac{1}{|\pi \tilde{\mathbf{C}}_k|} \exp \left(-(\mathbf{z}_k + \sqrt{p_u} M d_k \mathbf{u}_k)^H \tilde{\mathbf{C}}_k^{-1} (\mathbf{z}_k + \sqrt{p_u} M d_k \mathbf{u}_k) \right) \quad (20)$$

$P_{F,k} = P_f, \forall k$, the test statistic in (22) is reduced to $T_{C,I}(\mathbf{Z}) = \sum_{k=1}^K d_k \Re(\mathbf{z}_k^H \mathbf{C}_k^{-1} \mathbf{u}_k)$. The analytical performance of the detector in (22) can be characterized as shown below.

Theorem 1. The probabilities of false alarm (P_{FA}) and correct detection (P_D) of the fusion rule $T_C(\mathbf{Z})$ in (22) for DD in the mmWave massive MIMO WSN with a centralized antenna topology are

$$P_{FA} = Q\left(\frac{\gamma' - \mu_{T_C|\mathcal{H}_0}}{\sigma_{T_C|\mathcal{H}_0}}\right), P_D = Q\left(\frac{\gamma' - \mu_{T_C|\mathcal{H}_1}}{\sigma_{T_C|\mathcal{H}_1}}\right), \quad (23)$$

where $\mu_{T_C|\mathcal{H}_0}, \mu_{T_C|\mathcal{H}_1}$ are the means and $\sigma_{T_C|\mathcal{H}_0}^2, \sigma_{T_C|\mathcal{H}_1}^2$ denote the variances under the hypotheses of \mathcal{H}_0 and \mathcal{H}_1 , respectively, which are obtained as

$$\mu_{T_C|\mathcal{H}_0} = \sum_{k=1}^K \sqrt{p_u} M a_k c_k d_k^2 \mathbf{u}_k^H \mathbf{C}_k^{-1} \mathbf{u}_k, \quad (24)$$

$$\mu_{T_C|\mathcal{H}_1} = \sum_{k=1}^K \sqrt{p_u} M a_k b_k d_k^2 \mathbf{u}_k^H \mathbf{C}_k^{-1} \mathbf{u}_k, \quad (25)$$

$$\sigma_{T_C|\mathcal{H}_0}^2 = \sum_{k=1}^K M d_k^2 a_k^2 \left(M p_u \xi_k + \frac{\sigma_w^2}{2} d_k \mathbf{u}_k^H \mathbf{C}_k^{-2} \mathbf{u}_k \right), \quad (26)$$

$$\sigma_{T_C|\mathcal{H}_1}^2 = \sum_{k=1}^K M d_k^2 a_k^2 \left(M p_u \zeta_k + \frac{\sigma_w^2}{2} d_k \mathbf{u}_k^H \mathbf{C}_k^{-2} \mathbf{u}_k \right), \quad (27)$$

where $\xi_k = \left(\frac{\beta_{\frac{1}{2}}^2}{L_k} \mathbb{E}\{|\alpha_k^{l_k}|^4\} - d_k^2 c_k^2 \right) (\mathbf{u}_k^H \mathbf{C}_k^{-1} \mathbf{u}_k)^2$, $\zeta_k = \left(\frac{\beta_{\frac{1}{2}}^2}{L_k} \mathbb{E}\{|\alpha_k^{l_k}|^4\} - d_k^2 b_k^2 \right) (\mathbf{u}_k^H \mathbf{C}_k^{-1} \mathbf{u}_k)^2$, $b_k = 2P_{D,k} - 1$ and $c_k = 2P_{F,k} - 1$.

Proof. Given in Appendix A in [1]. \square

B. Fusion Rule for D-MIMO Based WSN

For the subsequent analysis, a distributed mmWave massive MIMO WSN is considered with a circular layout. This is motivated by the fact that compared to other antenna array layouts, the circular topology requires less optical backhaul installation [8] and is also compatible with the existing infrastructure [7]. All the K FCs are assumed to be uniformly distributed on a circle of radius r such that $r_0 \ll r < R$, where R represents the cell radius and r_0 denotes the minimum distance of the FCs from the cell center [52]. Therefore, the polar coordinates of the j th FC, $1 \leq j \leq K$, can be expressed as

$$(d_j, \varphi_j) = \left(r, \frac{2\pi(j-1)}{K} \right). \quad (28)$$

The K sensors having polar coordinates of (ρ_k, ψ_k) , $1 \leq k \leq K$, are assumed to be uniformly and randomly distributed

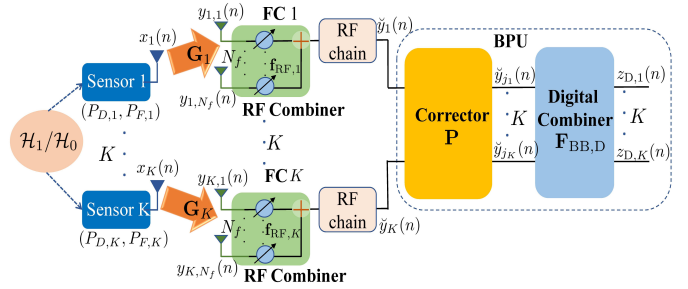


Figure 3. System model for distributed detection in a distributed configuration based mmWave massive MIMO WSN.

within the cell. The distance of the k th sensor from the j th FC, denoted by $\delta_{k,j}$, can be expressed as [52]

$$\delta_{k,j} = \sqrt{d_j^2 + \rho_k^2 - 2\rho_k d_j \cos(\psi_k - \varphi_j)}. \quad (29)$$

To further enhance the system performance, one can exploit the SINR- and D-selection methods for FC association [52]. Explicitly, the sensor selects the FC having the maximum SINR in the former, while in the latter it chooses the closest FC, i.e. the one with the minimum distance. However, typically D-selection is preferred due to its analytical tractability [52].

For D-selection, we can begin by constructing the distance matrix $\Delta \in \mathbb{C}^{K \times K}$, where $[\Delta]_{k,j} = \delta_{k,j}$, $1 \leq k \leq K$, $1 \leq j \leq K$. In each step, D-selection assigns sensor k to FC j , so that $[\Delta]_{k,j}$ is the minimum among the remaining entries of Δ . Post assignment, the entries $[\Delta]_{k,j}$ corresponding to sensor k and FC j are removed from the matrix and the process is repeated until all the sensors become associated. A correction matrix \mathbf{P} is employed to keep track of the associations, with $[\mathbf{P}]_{k,j} = 1$, when the k th sensor is connected to the j th FC, and 0 otherwise. Furthermore, \mathbf{P} has the property of $\mathbf{P}^H \mathbf{P} = \mathbf{I}_K$, since each sensor is associated with a single FC and vice-versa.

Consider now the composite observation matrix, $\tilde{\mathbf{Y}} = [\mathbf{Y}_1, \mathbf{Y}_2, \dots, \mathbf{Y}_K] \in \mathbb{C}^{N_f \times KN}$, constructed by concatenating the signal matrix \mathbf{Y}_j in (7) for all the K FCs. Exploiting the conditional independence of the observation matrices \mathbf{Y}_j , $1 \leq j \leq K$, corresponding to different FCs, the NP criterion based LLR test $T_D(\tilde{\mathbf{Y}})$ for DD in the massive D-MIMO sensor network can be formulated as

$$T_D(\tilde{\mathbf{Y}}) = \ln \left[\frac{p(\tilde{\mathbf{Y}}|\mathcal{H}_1)}{p(\tilde{\mathbf{Y}}|\mathcal{H}_0)} \right] = \ln \left[\frac{\prod_{j=1}^K p(\mathbf{Y}_j|\mathcal{H}_1)}{\prod_{j=1}^K p(\mathbf{Y}_j|\mathcal{H}_0)} \right] \underset{\mathcal{H}_0}{\overset{\mathcal{H}_1}{\gtrless}} \gamma, \quad (30)$$

where $p(\mathbf{Y}_j|\mathcal{H}_1)$, $p(\mathbf{Y}_j|\mathcal{H}_0)$ denote the PDFs of \mathbf{Y}_j under the hypotheses of \mathcal{H}_1 and \mathcal{H}_0 , respectively and γ represents the detection threshold. Exploiting the independence of $\mathbf{x}(n)$, $\forall n$, conditioned on the hypotheses \mathcal{H}_1 and \mathcal{H}_0 , the LLR test in (30) can be simplified to

$$T_D(\tilde{\mathbf{Y}}) = \sum_{j=1}^K \sum_{n=1}^N \ln \left[\frac{\sum_{\mathbf{x}(n)} p(\mathbf{y}_j(n)|\mathbf{x}(n)) \Pr(\mathbf{x}(n)|\mathcal{H}_1)}{\sum_{\mathbf{x}(n)} p(\mathbf{y}_j(n)|\mathbf{x}(n)) \Pr(\mathbf{x}(n)|\mathcal{H}_0)} \right] \quad (31)$$

$$= \sum_{j=1}^K \sum_{n=1}^N \ln \left[\frac{\sum_{\mathbf{x}(n)} \exp\left(-\frac{\|\mathbf{y}_j(n) - \sqrt{p_u} \mathbf{G}_j \mathbf{x}(n)\|^2}{\sigma_w^2}\right) \Pr(\mathbf{x}(n)|\mathcal{H}_1)}{\sum_{\mathbf{x}(n)} \exp\left(-\frac{\|\mathbf{y}_j(n) - \sqrt{p_u} \mathbf{G}_j \mathbf{x}(n)\|^2}{\sigma_w^2}\right) \Pr(\mathbf{x}(n)|\mathcal{H}_0)} \right]$$

The above expression is obtained by substituting the PDF of

$$p(\mathbf{y}_j(n)|\mathbf{x}(n)) = \frac{1}{(\pi\sigma_w^2)^{N_f}} \exp\left(-\frac{\|\mathbf{y}_j(n) - \sqrt{p_u} \mathbf{G}_j \mathbf{x}(n)\|^2}{\sigma_w^2}\right)$$

into (31). Similar to the C-MIMO setup, the test statistic above can be simplified as follows. In the first step, the observation matrix \mathbf{Y}_j is pre-processed at each FC using the RF combiner. The hybrid combining using the D-selection method first assigns the j th FC to the k_j -th sensor following the minimum distance criterion and then selects the l_{k_j} -th path of the channel between the j th FC and the k_j -th sensor by leveraging the small scale channel gain. Hence, the RF combiner $\mathbf{f}_{\text{RF},j} \in \mathbb{C}^{N_f \times 1}$ can be formulated as

$$\mathbf{f}_{\text{RF},j} = \mathbf{a}_r(\theta_{k_j,j}^{l_{k_j}}), \quad (32)$$

where $\mathbf{a}_r(\theta_{k_j,j}^{l_{k_j}})$ is the array response vector of the k_j th sensor, $1 \leq k_j \leq K$, for the l_{k_j} path with the maximum path gain $|\alpha_{k_j,j}^{l_{k_j}}|$ and $\theta_{k_j,j}^{l_{k_j}}$ is the corresponding AoA. The RF combiner outputs of all the K FCs are reordered using the correction matrix \mathbf{P} and subsequently processed at the BPU using the digital combiner $\mathbf{F}_{\text{BB},D} \in \mathbb{C}^{K \times K}$ to recover the soft decisions of each sensor, as demonstrated in Fig. 3. In the second step, all the sensor decisions are combined to arrive at the final decision. Utilizing the system model in (7), the RF combiner output $\check{\mathbf{y}}_j^T \in \mathbb{C}^{1 \times N}$ for the j th FC can be expressed as

$$\check{\mathbf{y}}_j^T = \sqrt{p_u} \mathbf{f}_{\text{RF},j}^H \mathbf{G}_j \mathbf{X} + \mathbf{f}_{\text{RF},j}^H \mathbf{W}_j. \quad (33)$$

The stacked RF combiner output $\check{\mathbf{Y}} = [\check{\mathbf{y}}_1, \check{\mathbf{y}}_2, \dots, \check{\mathbf{y}}_K]^T \in \mathbb{C}^{K \times N}$ corresponding to the K FCs is given in (34). Therefore, the equivalent system model obtained after applying the RF combiner can be formulated as

$$\check{\mathbf{Y}} = \sqrt{p_u} \mathbf{F}_{\text{RF},D}^H \mathbf{G}_D \mathbf{X} + \mathbf{F}_{\text{RF},D}^H \mathbf{W}_D, \quad (35)$$

where $\mathbf{F}_{\text{RF},D} = \text{diag}\{\mathbf{f}_{\text{RF},1}, \mathbf{f}_{\text{RF},2}, \dots, \mathbf{f}_{\text{RF},K}\} \in \mathbb{C}^{K N_f \times K}$ denotes the equivalent RF combiner and $\mathbf{G}_D = [\mathbf{G}_1^T, \mathbf{G}_2^T, \dots, \mathbf{G}_K^T]^T \in \mathbb{C}^{K N_f \times K}$, $\mathbf{W}_D = [\mathbf{W}_1^T, \mathbf{W}_2^T, \dots, \mathbf{W}_K^T]^T \in \mathbb{C}^{K N_f \times N}$ represent the stacked mmWave channel and noise matrices, respectively. The rearranged RF combiner output matrix $\mathbf{Y}_D = [\check{\mathbf{y}}_{j_1}, \check{\mathbf{y}}_{j_2}, \dots, \check{\mathbf{y}}_{j_K}]^T \in \mathbb{C}^{K \times N}$ can be expressed as

$$\mathbf{Y}_D = \sqrt{p_u} \mathbf{P} \mathbf{F}_{\text{RF},D}^H \mathbf{G}_D \mathbf{X} + \mathbf{P} \mathbf{F}_{\text{RF},D}^H \mathbf{W}_D, \quad (36)$$

where $\check{\mathbf{y}}_{j_k}^T$, $1 \leq j_k \leq K$, denotes the signal vector received at the j_k th FC associated with the k th sensor. Subsequently, the digital combiner $\mathbf{F}_{\text{BB},D} = \mathbf{P} \mathbf{F}_{\text{RF},D}^H \mathbf{G}_D \in \mathbb{C}^{K \times K}$ is employed to extract the outputs corresponding to each sensor. The resultant output matrix $\mathbf{Z}_D \in \mathbb{C}^{K \times N}$ can be expressed as

$$\mathbf{Z}_D = \sqrt{p_u} \mathbf{F}_{\text{BB},D}^H \mathbf{P} \mathbf{F}_{\text{RF},D}^H \mathbf{G}_D \mathbf{X} + \mathbf{F}_{\text{BB},D}^H \mathbf{P} \mathbf{F}_{\text{RF},D}^H \mathbf{W}_D. \quad (37)$$

It can be noted that the asymptotic orthogonality property of mmWave massive MIMO channels holds true also for the D-MIMO system [52], under the condition $L_{k,j} = o(N_f)$, $1 \leq k, j \leq K$, and can be expressed as

$$\mathbf{a}_r^H(\theta_{k,j}^{l_u}) \mathbf{a}_r(\theta_{s,t}^{l_v}) = \begin{cases} 1, & j = t \text{ and } k = s \text{ and } u = v \\ 0, & j \neq t \text{ or } k \neq s \text{ or } u \neq v \end{cases}. \quad (38)$$

Leveraging the above property and choosing the digital combiner matrix $\mathbf{F}_{\text{BB},D}$ to be diagonal [52] with its k th principal diagonal element given by $[\mathbf{F}_{\text{BB},D}]_{k,k} = \sqrt{\frac{N_f \beta_{k,j_k}}{L_{k,j_k}}} \alpha_{k,j_k}^{l_k}$, the hybrid combiner output $\mathbf{z}_{D,k} \in \mathbb{C}^{N \times 1}$ of the k th sensor can be determined as

$$\mathbf{z}_{D,k} = \sqrt{p_u} \frac{\beta_{k,j_k} N_f}{L_{k,j_k}} \left| \alpha_{k,j_k}^{l_k} \right|^2 \mathbf{x}_k + \tilde{\mathbf{w}}_{D,k}, \quad (39)$$

where $\tilde{\mathbf{w}}_{D,k} = \sqrt{\frac{N_f \beta_{k,j_k}}{L_{k,j_k}}} (\alpha_{k,j_k}^{l_k})^* (\mathbf{a}_r^H(\theta_{k,j_k}^{l_k}) \mathbf{W}_{j_k})^T \in \mathbb{C}^{N \times 1}$ represents the equivalent noise vector of the k th sensor, which obeys the complex Gaussian distribution $\tilde{\mathbf{w}}_{D,k} \sim \mathcal{CN}(\mathbf{0}, d_{k,j_k} \sigma_w^2 N_f \mathbf{I}_N)$ and $d_{k,j_k} \triangleq \frac{\beta_{k,j_k}}{L_{k,j_k}} \mathbb{E}\{|\alpha_{k,j_k}^{l_k}|^2\}$. Furthermore, the hybrid combiner output of the k th sensor $\mathbf{z}_{D,k}$ is also complex Normal distributed obeying $\mathbf{z}_{D,k} \sim \mathcal{CN}(\sqrt{p_u} N_f d_{k,j_k} \mathbf{x}_k, \mathbf{C}'_{D,k})$. Furthermore, the covariance matrix $\mathbf{C}'_{D,k} \in \mathbb{C}^{N \times N}$ of $\mathbf{z}_{D,k}$ can be formulated as $\mathbf{C}'_{D,k} = \frac{p_u N_f^2 \beta_{k,j_k}^2}{L_{k,j_k}^2} \text{var}\{|\alpha_{k,j_k}^{l_k}|^2\} \mathbf{x}_k \mathbf{x}_k^H + d_{k,j_k} \sigma_w^2 N_f \mathbf{I}_N$. Leveraging the conditional independence of the hybrid combiner outputs $\mathbf{z}_{D,k}$ across different sensors, the NP criterion based test statistic $T_D(\mathbf{Z})$ for DD in mmWave massive MIMO WSNs, relying on a distributed antenna topology can be formulated as

$$T_D(\mathbf{Z}_D) = \ln \left[\frac{p(\mathbf{Z}_D|\mathcal{H}_1)}{p(\mathbf{Z}_D|\mathcal{H}_0)} \right] = \ln \left[\prod_{k=1}^K \frac{p(\mathbf{z}_{D,k}|\mathcal{H}_1)}{p(\mathbf{z}_{D,k}|\mathcal{H}_0)} \right]. \quad (40)$$

The above test can be further simplified to the test statistic seen in (43), where (42) exploits the independence of the hybrid combiner outputs $\mathbf{z}_{D,k}$ of different sensors, given the transmit vectors of $\mathbf{x}_k \in \{\mathbf{u}_k, -\mathbf{u}_k\}$ for the antipodal signaling scheme. Substituting the PDFs of $\mathbf{z}_{D,k}$ corresponding to the local sensor decisions, which are given as

$$p(\mathbf{z}_{D,k}|\mathbf{x}_k = \mathbf{u}_k) \sim \mathcal{CN}(\sqrt{p_u} d_{k,j_k} N_f \mathbf{u}_k, \tilde{\mathbf{C}}_{D,k}), \quad (41)$$

$$p(\mathbf{z}_{D,k}|\mathbf{x}_k = -\mathbf{u}_k) \sim \mathcal{CN}(-\sqrt{p_u} d_{k,j_k} N_f \mathbf{u}_k, \tilde{\mathbf{C}}_{D,k}),$$

into (40) yields the expression of the test statistic in (43), where $\tilde{\mathbf{C}}_{D,k} = \frac{p_u N_f^2 \beta_{k,j_k}^2}{L_{k,j_k}^2} \text{var}\{|\alpha_{k,j_k}^{l_k}|^2\} \mathbf{u}_k \mathbf{u}_k^H + N_f d_{k,j_k} \sigma_w^2 \mathbf{I}_N = N_f \mathbf{C}_{D,k}$ and $\mathbf{C}_{D,k} = d_{k,j_k} \sigma_w^2 \mathbf{I}_N + \frac{p_u N_f \beta_{k,j_k}^2}{L_{k,j_k}^2} \text{var}\{|\alpha_{k,j_k}^{l_k}|^2\} \mathbf{u}_k \mathbf{u}_k^H$. Once again, at low SNR, the

$$\begin{bmatrix} \tilde{\mathbf{y}}_1^T \\ \tilde{\mathbf{y}}_2^T \\ \vdots \\ \tilde{\mathbf{y}}_K^T \end{bmatrix} = \sqrt{p_u} \begin{bmatrix} \mathbf{f}_{\text{RF},1}^H & \mathbf{0} & \cdots & \mathbf{0} \\ \mathbf{0} & \mathbf{f}_{\text{RF},2}^H & \cdots & \mathbf{0} \\ \vdots & \vdots & \ddots & \vdots \\ \mathbf{0} & \mathbf{0} & \cdots & \mathbf{f}_{\text{RF},K}^H \end{bmatrix} \begin{bmatrix} \mathbf{G}_1 \\ \mathbf{G}_2 \\ \vdots \\ \mathbf{G}_K \end{bmatrix} \mathbf{X} + \begin{bmatrix} \mathbf{f}_{\text{RF},1}^H & \mathbf{0} & \cdots & \mathbf{0} \\ \mathbf{0} & \mathbf{f}_{\text{RF},2}^H & \cdots & \mathbf{0} \\ \vdots & \vdots & \ddots & \vdots \\ \mathbf{0} & \mathbf{0} & \cdots & \mathbf{f}_{\text{RF},K}^H \end{bmatrix} \begin{bmatrix} \mathbf{W}_1 \\ \mathbf{W}_2 \\ \vdots \\ \mathbf{W}_K \end{bmatrix}, \quad (34)$$

$$T_D(\mathbf{Z}_D) = \sum_{k=1}^K \ln \left[\frac{p(\mathbf{z}_{D,k} | \mathbf{x}_k = \mathbf{u}_k) \Pr(\mathbf{x}_k = \mathbf{u}_k | \mathcal{H}_1) + p(\mathbf{z}_{D,k} | \mathbf{x}_k = -\mathbf{u}_k) \Pr(\mathbf{x}_k = -\mathbf{u}_k | \mathcal{H}_1)}{p(\mathbf{z}_{D,k} | \mathbf{x}_k = \mathbf{u}_k) \Pr(\mathbf{x}_k = \mathbf{u}_k | \mathcal{H}_0) + p(\mathbf{z}_{D,k} | \mathbf{x}_k = -\mathbf{u}_k) \Pr(\mathbf{x}_k = -\mathbf{u}_k | \mathcal{H}_0)} \right] \quad (42)$$

$$= \sum_{k=1}^K \ln \left[\frac{P_{D,k} + (1 - P_{D,k}) \exp(-4\sqrt{p_u} d_{k,j_k} \Re(\mathbf{z}_{D,k}^H \mathbf{C}_{D,k}^{-1} \mathbf{u}_k))}{P_{F,k} + (1 - P_{F,k}) \exp(-4\sqrt{p_u} d_{k,j_k} \Re(\mathbf{z}_{D,k}^H \mathbf{C}_{D,k}^{-1} \mathbf{u}_k))} \right], \quad (43)$$

above expression of $T_D(\mathbf{Z}_D)$ can be simplified to

$$T_D(\mathbf{Z}_D) = \sum_{k=1}^K a_k d_{k,j_k} \Re(\mathbf{z}_{D,k}^H \mathbf{C}_{D,k}^{-1} \mathbf{u}_k) \underset{\mathcal{H}_0}{\gtrsim} \tilde{\gamma}. \quad (44)$$

When $P_{D,k} = P_D$, $P_{F,k} = P_F$, $\forall k$, the test statistic in (44) further reduces to $T_{D,1}(\mathbf{Z}_D) = \sum_{k=1}^K d_{k,j_k} \Re(\mathbf{z}_{D,k}^H \mathbf{C}_{D,k}^{-1} \mathbf{u}_k)$. The theorem given below summarizes the performance of the test $T_D(\mathbf{Z}_D)$ for the null and alternative hypotheses.

Theorem 2. *The probabilities of false alarm (P_{FA}) and correct detection (P_D) of the detector in (44), using DD in our massive D-MIMO configuration, are formulated as*

$$P_{FA} = Q\left(\frac{\tilde{\gamma} - \mu_{T_D|\mathcal{H}_0}}{\sigma_{T_D|\mathcal{H}_0}}\right), P_D = Q\left(\frac{\tilde{\gamma} - \mu_{T_D|\mathcal{H}_1}}{\sigma_{T_D|\mathcal{H}_1}}\right), \quad (45)$$

where $\mu_{T_D|\mathcal{H}_0}$, $\mu_{T_D|\mathcal{H}_1}$ and $\sigma_{T_D|\mathcal{H}_0}^2$, $\sigma_{T_D|\mathcal{H}_1}^2$ represent the means and the variances of $T_D(\mathbf{Z}_D)$ corresponding to the hypotheses of \mathcal{H}_0 and \mathcal{H}_1 , respectively. The quantities $\mu_{T_D|\mathcal{H}_1}$ and $\sigma_{T_D|\mathcal{H}_1}^2$ are given by

$$\mu_{T_D|\mathcal{H}_1} = \sum_{k=1}^K \sqrt{p_u} N_f a_k b_k d_{k,j_k}^2 \mathbf{u}_k^H \mathbf{C}_{D,k}^{-1} \mathbf{u}_k, \quad (46)$$

$$\sigma_{T_D|\mathcal{H}_1}^2 = \sum_{k=1}^K a_k^2 d_{k,j_k}^2 N_f \left(p_u \zeta_{D,k} N_f + \frac{\sigma_w^2}{2} d_{k,j_k} \mathbf{u}_k^H \mathbf{C}_{D,k}^{-2} \mathbf{u}_k \right), \quad (47)$$

where $b_k = 2P_{D,k} - 1$ and $\zeta_{D,k} = \left(\frac{\beta_{k,j_k}^2}{L_{k,j_k}^2} \mathbb{E}\{|\alpha_{k,j_k}^{l_k}|^4\} - b_k^2 d_{k,j_k}^2 \right) (\mathbf{u}_k^H \mathbf{C}_{D,k}^{-1} \mathbf{u}_k)^2$. Similarly, the expressions of $\mu_{T_D|\mathcal{H}_0}$ and $\sigma_{T_D|\mathcal{H}_0}^2$ are

$$\mu_{T_D|\mathcal{H}_0} = \sum_{k=1}^K \sqrt{p_u} N_f a_k c_k d_{k,j_k}^2 \mathbf{u}_k^H \mathbf{C}_{D,k}^{-1} \mathbf{u}_k, \quad (48)$$

$$\sigma_{T_D|\mathcal{H}_0}^2 = \sum_{k=1}^K a_k^2 d_{k,j_k}^2 N_f \left(p_u \xi_{D,k} N_f + \frac{\sigma_w^2}{2} d_{k,j_k} \mathbf{u}_k^H \mathbf{C}_{D,k}^{-2} \mathbf{u}_k \right), \quad (49)$$

where $c_k = 2P_{F,k} - 1$ and $\xi_{D,k} = \left(\frac{\beta_{k,j_k}^2}{L_{k,j_k}^2} \mathbb{E}\{|\alpha_{k,j_k}^{l_k}|^4\} - d_{k,j_k}^2 c_k^2 \right) (\mathbf{u}_k^H \mathbf{C}_{D,k}^{-1} \mathbf{u}_k)^2$.

Proof. Given in Appendix A. \square

IV. LARGE-SCALE ANTENNA ARRAY ANALYSIS

Analytical expressions of the asymptotic probabilities of false alarm and correct detection are now obtained using an appropriate sensor power scaling law in the large-scale antenna regime to provide additional insights.

A. Large-Scale Antenna Array Analysis for a mmWave Massive C-MIMO WSN

For a C-MIMO WSN, consider the power scaling law $p_u = \frac{\tilde{p}_u}{M}$. The corresponding analytical expressions of the asymptotic detection performance of the fusion rule in (22) are now derived below for $p_u = \frac{\tilde{p}_u}{M}$.

Theorem 3. *The asymptotic probabilities of false alarm (P_{FA}^a) and correct detection (P_D^a) of the proposed detector in (22) for a centralized mmWave massive MIMO WSN, under the power scaling $p_u = \frac{\tilde{p}_u}{M}$ are formulated as*

$$P_{FA}^a = \lim_{M \rightarrow \infty} Q\left(\frac{\gamma' - \mu_{T_C|\mathcal{H}_0}}{\sigma_{T_C|\mathcal{H}_0}}\right) \Big|_{p_u = \frac{\tilde{p}_u}{M}} = Q(\gamma' - \mu_{T_C|\mathcal{H}_0}^a),$$

$$P_D^a = \lim_{M \rightarrow \infty} Q\left(\frac{\gamma' - \mu_{T_C|\mathcal{H}_1}}{\sigma_{T_C|\mathcal{H}_1}}\right) \Big|_{p_u = \frac{\tilde{p}_u}{M}} = Q(\gamma' - \mu_{T_C|\mathcal{H}_1}^a),$$

where the normalized means under the null and alternative hypotheses, denoted by $\mu_{T_C|\mathcal{H}_0}^a$ and $\mu_{T_C|\mathcal{H}_1}^a$, respectively, are expressed as

$$\mu_{T_C|\mathcal{H}_0}^a = \frac{\sum_{k=1}^K \sqrt{\tilde{p}_u} a_k c_k d_{k,j_k}^2 \mathbf{u}_k^H (\mathbf{C}_k^a)^{-1} \mathbf{u}_k}{\sqrt{\sum_{k=1}^K d_{k,j_k}^2 a_k^2 (\tilde{p}_u \zeta_k^a + \frac{\sigma_w^2}{2} d_{k,j_k} \mathbf{u}_k^H (\mathbf{C}_k^a)^{-2} \mathbf{u}_k)}}, \quad (50)$$

$$\mu_{T_C|\mathcal{H}_1}^a = \frac{\sum_{k=1}^K \sqrt{\tilde{p}_u} a_k b_k d_{k,j_k}^2 \mathbf{u}_k^H (\mathbf{C}_k^a)^{-1} \mathbf{u}_k}{\sqrt{\sum_{k=1}^K d_{k,j_k}^2 a_k^2 (\tilde{p}_u \zeta_k^a + \frac{\sigma_w^2}{2} d_{k,j_k} \mathbf{u}_k^H (\mathbf{C}_k^a)^{-2} \mathbf{u}_k)}}, \quad (51)$$

where we have $\zeta_k^a = \left(\frac{\beta_{k,j_k}^2}{L_{k,j_k}^2} \mathbb{E}\{|\alpha_{k,j_k}^{l_k}|^4\} - d_{k,j_k}^2 b_k^2 \right) (\mathbf{u}_k^H (\mathbf{C}_k^a)^{-1} \mathbf{u}_k)^2$, $\xi_k^a = \left(\frac{\beta_{k,j_k}^2}{L_{k,j_k}^2} \mathbb{E}\{|\alpha_{k,j_k}^{l_k}|^4\} - d_{k,j_k}^2 c_k^2 \right) (\mathbf{u}_k^H (\mathbf{C}_k^a)^{-1} \mathbf{u}_k)^2$ and $\mathbf{C}_k^a = \frac{\tilde{p}_u \beta_{k,j_k}^2}{L_{k,j_k}^2} \text{var}\{|\alpha_{k,j_k}^{l_k}|^2\} \mathbf{u}_k \mathbf{u}_k^H + \sigma_w^2 d_{k,j_k} \mathbf{I}_N$.

Proof. Given in Appendix B. \square

The asymptotic performance of a D-MIMO based WSN is discussed next. \square

B. Large-Scale Antenna Array Analysis for a mmWave Massive D-MIMO WSN

For the D-MIMO configuration, consider the power scaling law $p_u = \frac{\tilde{p}_u}{N_f}$. The asymptotic probabilities of false alarm (P_{FA}^a) and correct detection (P_D^a) under this scaling law are presented in the following theorem.

Theorem 4. *The asymptotic P_{FA}^a and P_D^a of the test statistic in (44) for a mmWave massive D-MIMO WSN, under the power scaling $p_u = \frac{\tilde{p}_u}{N_f}$, are given as*

$$P_{FA}^a = \lim_{N_f \rightarrow \infty} Q\left(\frac{\tilde{\gamma} - \mu_{T_D|\mathcal{H}_0}}{\sigma_{T_D|\mathcal{H}_0}}\right)\Bigg|_{p_u = \frac{\tilde{p}_u}{N_f}} = Q(\tilde{\gamma} - \mu_{T_D}^a|\mathcal{H}_0),$$

$$P_D^a = \lim_{N_f \rightarrow \infty} Q\left(\frac{\tilde{\gamma} - \mu_{T_D|\mathcal{H}_1}}{\sigma_{T_D|\mathcal{H}_1}}\right)\Bigg|_{p_u = \frac{\tilde{p}_u}{N_f}} = Q(\tilde{\gamma} - \mu_{T_D}^a|\mathcal{H}_1),$$

where the quantities $\mu_{T_D}^a|\mathcal{H}_0$ and $\mu_{T_D}^a|\mathcal{H}_1$ represent the normalized means pertaining to the null and alternative hypotheses, respectively, which are derived as

$$\mu_{T_D}^a|\mathcal{H}_0 = \frac{\sum_{k=1}^K \sqrt{\tilde{p}_u} a_k c_k d_{k,j_k}^2 \mathbf{u}_k^H (\mathbf{C}_{D,k}^a)^{-1} \mathbf{u}_k}{\sqrt{\sum_{k=1}^K d_{k,j_k}^2 a_k^2 \left(\tilde{p}_u \zeta_{D,k}^a + \frac{\sigma_w^2}{2} d_{k,j_k} \mathbf{u}_k^H (\mathbf{C}_{D,k}^a)^{-2} \mathbf{u}_k\right)}}, \quad (52)$$

$$\mu_{T_D}^a|\mathcal{H}_1 = \frac{\sum_{k=1}^K \sqrt{\tilde{p}_u} a_k b_k d_{k,j_k}^2 \mathbf{u}_k^H (\mathbf{C}_{D,k}^a)^{-1} \mathbf{u}_k}{\sqrt{\sum_{k=1}^K d_{k,j_k}^2 a_k^2 \left(\tilde{p}_u \zeta_{D,k}^a + \frac{\sigma_w^2}{2} d_{k,j_k} \mathbf{u}_k^H (\mathbf{C}_{D,k}^a)^{-2} \mathbf{u}_k\right)}}. \quad (53)$$

The various quantities used above are defined as $\zeta_{D,k}^a = \left(\frac{\beta_{k,j_k}^2}{L_{k,j_k}^2} \mathbb{E}\{|\alpha_{k,j_k}^{l_k}|^4\} - d_{k,j_k}^2 b_k^2\right) (\mathbf{u}_k^H (\mathbf{C}_{D,k}^a)^{-1} \mathbf{u}_k)^2$ and $\xi_{D,k}^a = \left(\frac{\beta_{k,j_k}^2}{L_{k,j_k}^2} \mathbb{E}\{|\alpha_{k,j_k}^{l_k}|^4\} - d_{k,j_k}^2 c_k^2\right) (\mathbf{u}_k^H (\mathbf{C}_{D,k}^a)^{-1} \mathbf{u}_k)^2$ with $\mathbf{C}_{D,k}^a = \frac{\tilde{p}_u \beta_{k,j_k}^2}{L_{k,j_k}^2} \text{var}\{|\alpha_{k,j_k}^{l_k}|^2\} \mathbf{u}_k \mathbf{u}_k^H + \sigma_w^2 d_{k,j_k} \mathbf{I}_N$.

Proof. Follows similar lines to that of Theorem 3 in Appendix B. \square

The results in Theorem 3 and Theorem 4 have significant implications for the practical deployment of mmWave massive MIMO sensor networks, since they demonstrate that the sensors may significantly reduce their energy consumption, proportional to $1/M$ and $1/N_f$ for the C- and D-MIMO configurations, respectively, without any performance degradation. This in turn results in prolonged battery life of the sensors, ensuring reliable WSN operation.

V. TRANSMIT SIGNALING MATRICES

This section develops an optimization framework for finding the optimal signaling matrices $\mathbf{X} = [\mathbf{x}_1, \mathbf{x}_2, \dots, \mathbf{x}_K]^T \in \mathbb{C}^{K \times N}$, that enhance the detection performance of the fusion rules proposed in Section III. Consider a column wise stacking of the matrix $\mathbf{U}^T = [\mathbf{u}_1, \mathbf{u}_2, \dots, \mathbf{u}_K]$ to obtain the vector

$\mathbf{u} \in \mathbb{C}^{KL \times 1}$, described as $\mathbf{u} = \text{vec}(\mathbf{U}^T)$. The detection performance of the sensor network can be boosted by maximizing the deflection coefficient $d^2(\mathbf{u})$ [49], expressed as

$$d^2(\mathbf{u}) = \frac{(\mu_{T|\mathcal{H}_1} - \mu_{T|\mathcal{H}_0})^2}{\sigma_{T|\mathcal{H}_0}^2}, \quad (54)$$

where $\mu_{T|\mathcal{H}_1}$, $\mu_{T|\mathcal{H}_0}$ denote the means of the test $T(\mathbf{Z})$ under the alternative and null hypotheses, respectively, and $\sigma_{T|\mathcal{H}_0}^2$ is the variance under the null hypothesis. The signaling matrices of the centralized and distributed antenna configurations are determined next.

A. Signaling Matrix Design for a C-MIMO System

Using (54) and the expressions of $\mu_{T_C|\mathcal{H}_0}$, $\mu_{T_C|\mathcal{H}_1}$ and $\sigma_{T_C|\mathcal{H}_0}^2$ given in Theorem 1, the deflection coefficient $d_C^2(\mathbf{u})$ for the C-MIMO system can be formulated as

$$d_C^2(\mathbf{u}) = \frac{(\mu_{T_C|\mathcal{H}_1} - \mu_{T_C|\mathcal{H}_0})^2}{\sigma_{T_C|\mathcal{H}_0}^2} = \frac{\left(\sum_{k=1}^K \sqrt{\tilde{p}_u} M d_k^2 a_k (b_k - c_k) \mathbf{u}_k^H \mathbf{C}_k^{-1} \mathbf{u}_k\right)^2}{\sum_{k=1}^K M d_k^2 a_k^2 \left(M p_u \xi_k + \frac{\sigma_w^2}{2} d_k \mathbf{u}_k^H \mathbf{C}_k^{-2} \mathbf{u}_k\right)}, \quad (55)$$

where ξ_k is defined in Theorem 1. To simplify the above expression, one can define the block-diagonal matrices of $\mathbf{\Lambda}_N \in \mathbb{C}^{KN \times KN}$, $\mathbf{\Omega}_N \in \mathbb{C}^{KN \times KN}$ and $\mathbf{\Gamma}_N \in \mathbb{C}^{KN \times KN}$ with block diagonal elements of $[\mathbf{\Lambda}_N]_k = [\mathbf{\Lambda}]_{k,k} \mathbf{C}_k^{-1}$, $[\mathbf{\Omega}_N]_k = [\mathbf{\Omega}]_{k,k} \mathbf{C}_k^{-1}$ and $[\mathbf{\Gamma}_N]_k = [\mathbf{\Gamma}]_{k,k} \mathbf{C}_k^{-2}$, respectively, where we have

$$[\mathbf{\Lambda}]_{k,k} = \sqrt{\tilde{p}_u} M d_k^2 a_k (b_k - c_k), [\mathbf{\Gamma}]_{k,k} = \frac{\sigma_w^2}{2} M d_k^3 a_k^2,$$

$$[\mathbf{\Omega}]_{k,k} = \sqrt{\tilde{p}_u} M d_k a_k \sqrt{\frac{\beta_k^2}{L_k^2} \mathbb{E}\{|\alpha_k^{l_k}|^4\} - c_k^2 d_k^2}. \quad (56)$$

Using the above quantities, the deflection coefficient expression in (55) can be closely approximated as

$$d^2(\mathbf{u}) \approx \frac{(\mathbf{u}^H \mathbf{\Lambda}_N \mathbf{u})^2}{(\mathbf{u}^H \mathbf{\Omega}_N \mathbf{u})^2 + \mathbf{u}^H \mathbf{\Gamma}_N \mathbf{u}}. \quad (57)$$

Since the expression in (57) is non-convex, direct maximization of the deflection coefficient is challenging. Hence, for obtaining a tractable solution, the original objective function can be recast as

$$\max_{\mathbf{u}} \frac{\mathbf{u}^H (\mathbf{\Lambda}_N \mathbf{u} \mathbf{u}^H \mathbf{\Lambda}_N) \mathbf{u}}{\mathbf{u}^H (\mathbf{\Omega}_N \mathbf{u} \mathbf{u}^H \mathbf{\Omega}_N + \mathbf{\Gamma}_N) \mathbf{u}} = \max_{\mathbf{u}} \frac{\mathbf{u}^H \mathbf{\Psi} \mathbf{u}}{\mathbf{u}^H \mathbf{\Xi} \mathbf{u}}, \quad (58)$$

where $\mathbf{\Xi} = \mathbf{\Omega}_N \mathbf{u} \mathbf{u}^H \mathbf{\Omega}_N + \mathbf{\Gamma}_N$ and $\mathbf{\Psi} = \mathbf{\Lambda}_N \mathbf{u} \mathbf{u}^H \mathbf{\Lambda}_N$. Using the standard form of the Rayleigh quotient of [53], the objective function in (58) can be similarly modified as

$$\max_{\mathbf{u}} \frac{\mathbf{u}^H \mathbf{\Psi} \mathbf{u}}{\mathbf{u}^H \mathbf{\Xi}^{1/2} \mathbf{\Xi}^{1/2} \mathbf{u}} = \max_{\mathbf{v}} \frac{\mathbf{v}^H \mathbf{\Xi}^{-1/2} \mathbf{\Psi} \mathbf{\Xi}^{-1/2} \mathbf{v}}{\mathbf{v}^H \mathbf{v}} = \max_{\mathbf{v}} \frac{\mathbf{v}^H \mathbf{A} \mathbf{v}}{\mathbf{v}^H \mathbf{v}}, \quad (59)$$

where $\mathbf{v} = \mathbf{\Xi}^{1/2} \mathbf{u}$ and $\mathbf{A} = \mathbf{\Xi}^{-1/2} \mathbf{\Psi} \mathbf{\Xi}^{-1/2}$. The above optimization problem can be solved iteratively for determining

the optimal signal vector \mathbf{u} and the solution for the l th iteration is determined below.

Theorem 5. For a centralized antenna topology, the transmit signaling matrix $\mathbf{U}^{(l)}$ in the l th iteration can be derived as $\mathbf{U}^{(l)} = (\text{vec}^{-1}(\mathbf{u}^{(l)}))^T = (\text{vec}^{-1}((\Xi^{(l-1)})^{-1/2} \mathbf{v}^{(l)}))^T$, where $\mathbf{v}^{(l)}$ is the solution of the optimization problem below

$$\max_{\mathbf{v}^{(l)}} \frac{\mathbf{v}^{(l)H} \mathbf{A}^{(l-1)} \mathbf{v}^{(l)}}{\mathbf{v}^{(l)H} \mathbf{v}^{(l)}}, \quad (60)$$

with $\mathbf{A}^{(l-1)} = (\Xi^{(l-1)})^{-1/2} \Psi^{(l-1)} (\Xi^{(l-1)})^{-1/2}$, $\mathbf{v}^{(l)} = (\Xi^{(l-1)})^{1/2} \mathbf{u}^{(l)}$. The matrices $\Xi^{(l-1)}$ and $\Psi^{(l-1)}$ are determined upon replacing \mathbf{u} by $\mathbf{u}^{(l-1)}$ in (58).

It can be readily seen that the solution $\mathbf{v}^{(l)}$ of the optimization problem in (60) is given by $\mathbf{v}^{(l)} = \alpha \mathbf{v}_m^{(l-1)}$, where α denotes the scaling factor for the total power and $\mathbf{v}_m^{(l-1)}$ is the eigenvector of the matrix $\mathbf{A}^{(l-1)}$ corresponding to its maximum eigenvalue. The vector \mathbf{u} is initialized as $\mathbf{u}^{(0)} = \text{vec}((\mathbf{U}^{(0)})^T)$, where the transmit signaling matrix $\mathbf{U}^{(0)}$ at the 0th iteration is chosen as a semi-unitary matrix defined in [17]. Consequently, the transmit signaling matrix during the l th iteration can be formulated as $\mathbf{U}^{(l)} = (\text{vec}^{-1}((\Xi^{(l-1)})^{-1/2} \mathbf{v}^{(l)}))^T$, which further enhances the performance of the detector proposed in (22) for a mmWave massive MIMO based WSN relying on centralized antenna configuration.

B. Signaling Matrix Design for a D-MIMO System

For a D-MIMO topology, the deflection coefficient $d_{\mathbf{u}_D}^2$ [49] of the test statistic in (44) can be approximated as

$$\begin{aligned} d^2(\mathbf{u}_D) &= \frac{(\mu_{T_b|\mathcal{H}_1} - \mu_{T_b|\mathcal{H}_0})^2}{\sigma_{T_b|\mathcal{H}_0}^2} \\ &= \frac{\left(\sum_{k=1}^K \sqrt{p_u} N_f d_{k,j_k}^2 a_k (b_k - c_k) \mathbf{u}_k^H \mathbf{C}_{D,k}^{-1} \mathbf{u}_k \right)^2}{\sum_{k=1}^K N_f d_{k,j_k}^2 a_k^2 \left(N_f p_u \xi_{D,k} + \frac{\sigma_w^2}{2} d_{k,j_k} \mathbf{u}_k^H \mathbf{C}_{D,k}^{-2} \mathbf{u}_k \right)} \\ &\approx \frac{(\mathbf{u}_D^H \mathbf{\Lambda}_{D,N} \mathbf{u}_D)^2}{(\mathbf{u}_D^H \mathbf{\Omega}_{D,N} \mathbf{u}_D)^2 + \mathbf{u}_D^H \mathbf{\Gamma}_{D,N} \mathbf{u}_D}, \end{aligned} \quad (61)$$

where the expressions of $\mu_{T_b|\mathcal{H}_1}$, $\mu_{T_b|\mathcal{H}_0}$ and $\sigma_{T_b|\mathcal{H}_0}^2$ are given in (46), (48) and (49), respectively. The block diagonal components of the matrices $\mathbf{\Lambda}_{D,N}$, $\mathbf{\Omega}_{D,N}$ and $\mathbf{\Gamma}_{D,N}$ are defined as $[\mathbf{\Lambda}_{D,N}]_k = [\mathbf{\Lambda}_D]_{k,k} \mathbf{C}_{D,k}^{-1}$, $[\mathbf{\Omega}_{D,N}]_k = [\mathbf{\Omega}_D]_{k,k} \mathbf{C}_{D,k}^{-1}$ and $[\mathbf{\Gamma}_{D,N}]_k = [\mathbf{\Theta}_D]_{k,k} \mathbf{C}_{D,k}^{-2}$, respectively. Furthermore, $[\mathbf{\Lambda}_D]_{k,k}$, $[\mathbf{\Omega}_D]_{k,k}$ and $[\mathbf{\Theta}_D]_{k,k}$ can be derived from (56) upon replacing M and d_k by N_f and d_{k,j_k} , respectively. Following similar lines to those of Theorem 5, the objective function in (61) can be equivalently expressed as

$$\max_{\mathbf{u}_D} \frac{\mathbf{u}_D^H \Psi_D \mathbf{u}_D}{\mathbf{u}_D^H \Xi_D \mathbf{u}_D} = \max_{\mathbf{v}_D} \frac{\mathbf{v}_D^H \mathbf{A}_D \mathbf{v}_D}{\mathbf{v}_D^H \mathbf{v}_D}, \quad (62)$$

where the matrices obey $\mathbf{A}_D = \Xi_D^{-1/2} \Psi_D \Xi_D^{-1/2}$, $\Psi_D = \mathbf{\Lambda}_{D,N} \mathbf{u}_D \mathbf{u}_D^H \mathbf{\Lambda}_{D,N}$, $\Xi_D = \mathbf{\Omega}_{D,N} \mathbf{u}_D \mathbf{u}_D^H \mathbf{\Omega}_{D,N} + \mathbf{\Gamma}_{D,N}$ and $\mathbf{v}_D = \Xi_D^{1/2} \mathbf{u}_D$. The optimization problem in (62) can be solved iteratively and the transmit signaling matrix $\mathbf{U}_D^{(l)}$ during the l th

Table II
SPECIFICATION OF NUMERICAL PARAMETERS

Parameters	Values
A priori probability of \mathcal{H}_1 : $\Pr(\mathcal{H}_1)$	1/2
A priori probability of \mathcal{H}_0 : $\Pr(\mathcal{H}_0)$	1/2
Carrier frequency: f_c	28 GHz
Inter-antenna spacing: d	0.5λ
Noise variance: σ_w^2	1
Number of sensors: K	12
Maximum no. of propagation paths: L_m	10
Minimum distance between sensor and FC: r_0	1m
Cell radius and Path loss exponent: R, ν	200 m, 2
Mean and standard deviation of shadowing factor: μ_q, σ_q	4 dB, 2 dB
Radius of all the FCs: r	$0.6R$

iteration is given by $\mathbf{U}_D^{(l)} = (\text{vec}^{-1}[\eta (\Xi_D^{(l-1)})^{-1/2} \mathbf{v}_m^{(l-1)}])^T$, where $\mathbf{v}_m^{(l-1)}$ is the eigenvector of the matrix $\mathbf{A}_D^{(l-1)}$ corresponding to the maximum eigenvalue and η denotes the scaling coefficient used for meeting the total power constraint. The probability of error of the proposed detectors is derived next.

VI. ANALYSIS OF ERROR PROBABILITY

This section characterizes the probability of error of the detectors proposed in (22) and (44). Consider the a priori probabilities of both the hypotheses $\Pr(\mathcal{H}_1)$, $\Pr(\mathcal{H}_0)$ to be given as $\Pr(\mathcal{H}_1) = \epsilon$ and $\Pr(\mathcal{H}_0) = 1 - \epsilon$, respectively. The conditional probabilities $\Pr(\mathcal{H}_1|\mathcal{H}_0)$ and $\Pr(\mathcal{H}_0|\mathcal{H}_1)$ are given as P_{FA} and $1 - P_D$, respectively. Hence, the probability of error P_e can in turn be determined as [49],

$$\begin{aligned} P_e &= \Pr(\mathcal{H}_0|\mathcal{H}_1) \Pr(\mathcal{H}_1) + \Pr(\mathcal{H}_1|\mathcal{H}_0) \Pr(\mathcal{H}_0) \\ &= (1 - P_D) \epsilon + P_{FA} (1 - \epsilon). \end{aligned} \quad (63)$$

Upon substituting the expressions of P_D and P_{FA} , from (23), into (63), the expression of P_e for the C-MIMO configuration can be formulated as

$$P_e = \epsilon \left(1 - Q \left(\frac{\gamma' - \mu_{T_c|\mathcal{H}_1}}{\sigma_{T_c|\mathcal{H}_1}} \right) \right) + (1 - \epsilon) Q \left(\frac{\gamma' - \mu_{T_c|\mathcal{H}_0}}{\sigma_{T_c|\mathcal{H}_0}} \right), \quad (64)$$

where $\mu_{T_c|\mathcal{H}_1}$, $\mu_{T_c|\mathcal{H}_0}$, $\sigma_{T_c|\mathcal{H}_1}$ and $\sigma_{T_c|\mathcal{H}_0}$ are defined in Theorem 1. Similarly, upon substituting P_D and P_{FA} , from (45), into (63), the expression of P_e for the D-MIMO system, can be derived as

$$P_e = \epsilon \left(1 - Q \left(\frac{\tilde{\gamma} - \mu_{T_b|\mathcal{H}_1}}{\sigma_{T_b|\mathcal{H}_1}} \right) \right) + (1 - \epsilon) Q \left(\frac{\tilde{\gamma} - \mu_{T_b|\mathcal{H}_0}}{\sigma_{T_b|\mathcal{H}_0}} \right), \quad (65)$$

where $\mu_{T_b|\mathcal{H}_1}$, $\mu_{T_b|\mathcal{H}_0}$, $\sigma_{T_b|\mathcal{H}_1}$ and $\sigma_{T_b|\mathcal{H}_0}$ are given in Theorem 2. Our simulation results are presented next for quantifying the performance of the proposed detectors.

VII. SIMULATION RESULTS

In our simulations, K sensors are assumed to be uniformly and randomly distributed in an annular region with maximum distance of R and minimum distance of r_0 for the C-MIMO system. For the D-MIMO system, the sensors are uniformly and randomly distributed within the range of $\Sigma = [0, r - r_0] \cup [r + r_0, R]$, where r is the radius of a circle on which multiple

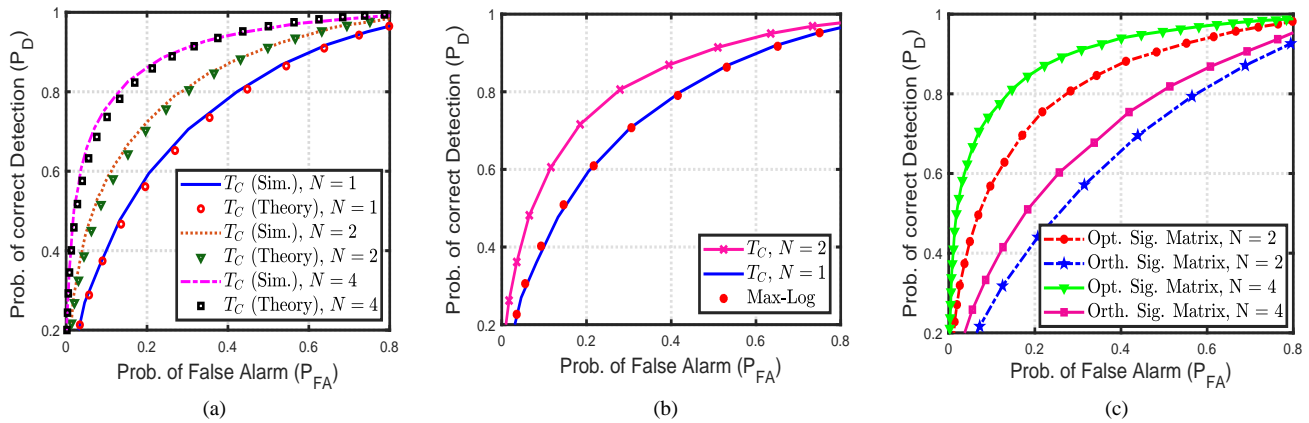


Figure 4. P_D vs. P_{FA} plot for $M = 250$ and $p_u = -18$ dB for comparing (a) simulated and analytical performance of the test $T_C(\mathbf{Z})$ in (22) for $N \in \{1, 2, 4\}$, (b) the detection performance of the test in (22) for $N \in \{1, 2\}$ with Max-log detector, (c) the C-MIMO detector employing the orthogonal signaling matrix and improved signaling matrix derived in Theorem 5 for $N \in \{2, 4\}$.

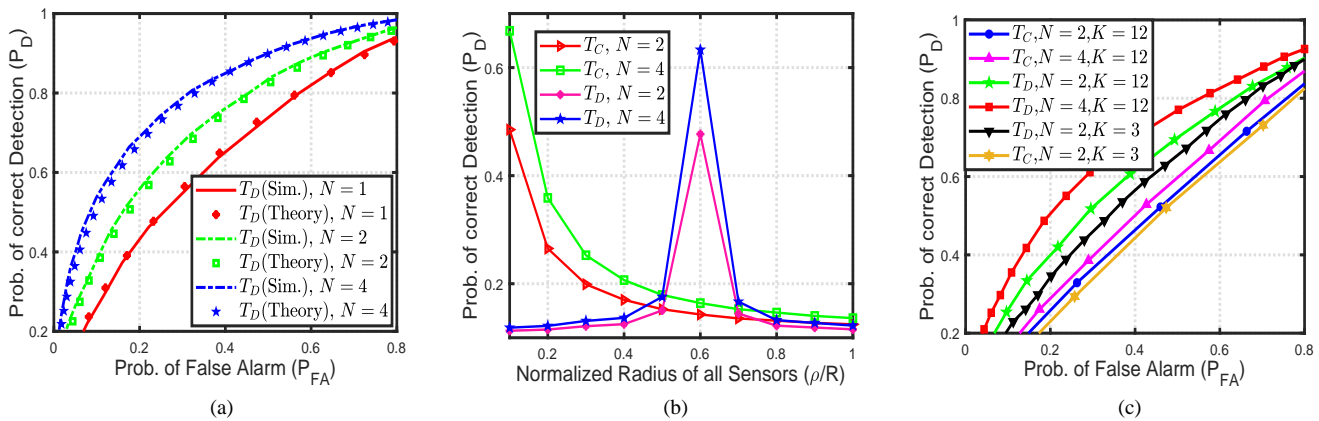


Figure 5. For parameters $p_u = -18$ dB, $N_f = 40$, $N_{tot} = M = 480$, (a) P_D vs. P_{FA} plot for verifying the analytical results of the test $T_D(\mathbf{Z}_D)$ in (44) for $N \in \{1, 2, 4\}$, (b) P_D vs. normalized sensor radius $\frac{\rho}{R}$ for C- and D-MIMO systems with $P_{FA} = 0.1$ and $N \in \{2, 4\}$, (c) P_D vs. P_{FA} plot for D- and C-MIMO systems with the sensors distributed uniformly in the range $[0.5R, R]$ with $N_f = 40$, $K = 12$, $N \in \{2, 4\}$ and $N_f = 160$, $K = 3$, $N = 2$.

FCs are deployed, similar to the model in [52]. Furthermore, it is assumed that the local detection metrics are distributed as $P_{D,k} \sim \mathcal{U}[0.40, 0.95]$ and $P_{F,k} \sim \mathcal{U}[0.01, 0.12]$, respectively.

Similar to [6], the large-scale fading coefficients $\beta_k, \beta_{k,j}$ for the centralized and distributed configurations are generated as $\beta_k = \frac{q_k}{(r_k/r_0)^\nu}$ and $\beta_{k,j} = \frac{q_{k,j}}{(\delta_{k,j}/r_0)^\nu}$, respectively, where $q_k, q_{k,j}$ are log-normal random variables having a mean of μ_q and standard deviation of σ_q , r_k is the distance of the k th sensor from the FC for the centralized antenna topology, while $\delta_{k,j}$ denotes its counterpart in the distributed antenna topology. Furthermore, ν is the path-loss exponent. The various parameters utilized for generating the simulation results along with their numerical values are specified in Table II.

Fig. 4a portrays the P_D vs. P_{FA} performance of the detector proposed in (22) along with the corresponding analytical values obtained using the expressions determined in Theorem 1 for the C-MIMO configuration. The ROC curves are given for various values of the transmit duration $N \in \{1, 2, 4\}$. It can be observed that the plots obtained via simulation are in close agreement with their analytical counterparts, thus

validating the theoretical expression in Theorem 1. Furthermore, the performance improves upon increasing N . Fig. 4b examines the detection performance of the simplified fusion rule of (22) for $N \in \{1, 2\}$ and compares it to the Max-Log detector that applies hybrid combining to the received signal and subsequently employs the Max-Log principle [16]. It is evident that the proposed detector outperforms the near-optimal Max-Log detector. Fig. 4c also demonstrates the impact of employing the improved signaling matrix derived in Theorem 5 for the C-MIMO configuration, which can be seen to lead to a considerably improved detection performance in comparison to a conventional orthogonal transmit signaling matrix. Further, Fig. 7 demonstrates the convergence of $\|\mathbf{u}^l\|^2$ to a constant value for increasing l .

Fig. 5a presents a similar comparison of the detector in (44) for the D-MIMO setup with the corresponding analytical results obtained in Theorem 2, which are seen to be in close agreement. In Fig. 5b, Fig. 6b, Fig. 8 and Fig. 9, we analyze the effect of varying other parameters, such as the normalized radius ρ/R of all sensors, total number of antennas N_{tot} ,

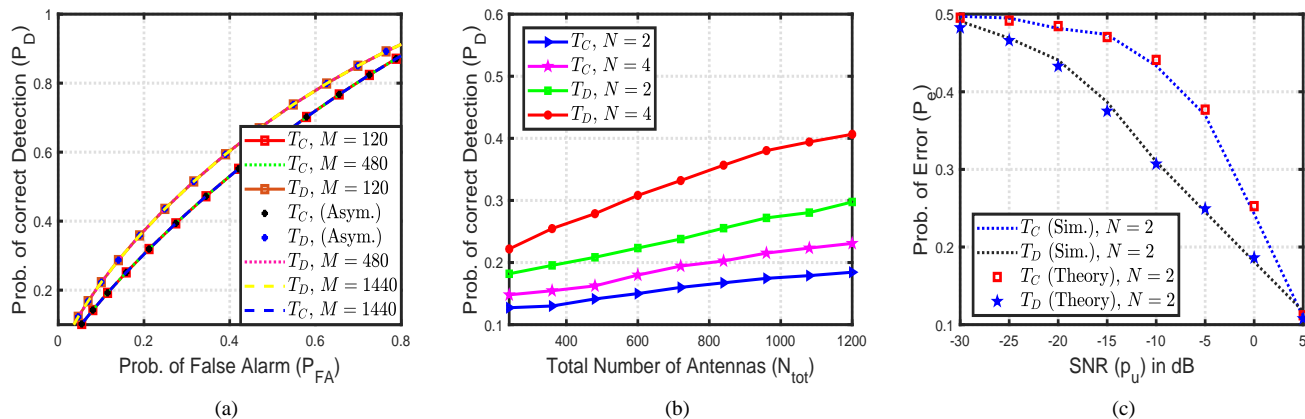


Figure 6. For the C- and D-MIMO detectors in (22) and (44), respectively, when the sensors are uniformly distributed in the range $[0.5R, R]$, (a) P_D vs. P_{FA} large-scale antenna array results for $N_{tot} = M \in \{120, 480, 1440\}$, $p_u = -10$ dB and $N = 4$ (b) P_D vs. total number of FC antennas N_{tot} for $p_u = -18$ dB, $P_{FA} = 0.1$ and $N \in \{2, 4\}$, (c) Probability of error P_e vs. SNR p_u for $N_{tot} = 600$, $P_{FA} = 0.1$ and $N = 2$.

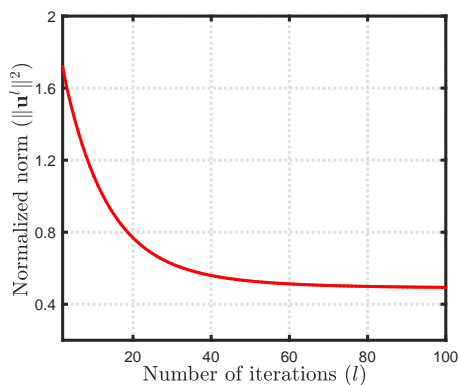


Figure 7. Normalized norm $\|\mathbf{u}^l\|^2$ vs. number of iterations l to demonstrate the convergence of Theorem 5.

total number of sensors K and path loss exponent ν , respectively, on the probability of detection P_D while maintaining a fixed probability of false alarm P_{FA} . Fig. 5b shows the probability of correct detection versus the normalized radius of all the sensors $\frac{\rho}{R}$ for the detectors proposed in (22) and (44) corresponding to the centralized and distributed antenna architectures, respectively. The other parameters are chosen as $P_{FA} = 0.1$, $N \in \{2, 4\}$ and $N_{tot} = M = 480$. All K sensors are assumed to be randomly and uniformly distributed on a circle of radius ρ , such that $r_k = \rho_k = \rho, \forall k$. It can be observed that the D-MIMO detector of (44) yields an improved performance compared to the C-MIMO detector of (22) for $\frac{\rho}{R}$ in the range $0.5 \leq \frac{\rho}{R} \leq 0.8$, which peaks at $\rho = 0.6R$. This interesting observation can be attributed to the fact that sensors are closest to their allocated FCs for $\rho = 0.6R$ in the D-MIMO setup, thus resulting in a significantly higher performance gain for $\frac{\rho}{R}$ around 0.6. Fig. 5c compares the P_D vs. P_{FA} plots of the D-MIMO and C-MIMO detectors for $N \in \{2, 4\}$, when the sensors are uniformly and randomly distributed in the range $[0.5R, R]$. This clearly demonstrates the fact that the D-MIMO performance is improved in comparison to that of C-MIMO detectors, when the sensors are located closer

to the cell edge and farther from the cell centre, which is in conformance with the trend seen in Fig. 5b. Furthermore, it should be noted that the distributed antenna architecture performs better than the centralized architecture even for $K = 3$.

Fig. 6a visualizes the analytical outcomes of the large-scale antenna array analysis of Section IV for the detectors proposed for the different antenna configurations, when the sensors are uniformly distributed in the range $[0.5R, R]$. The P_D vs P_{FA} plots of both the systems converge to their corresponding asymptotic bounds, determined in Theorem 3 and Theorem 4, respectively, when the sensor transmit power is scaled as $p_u = \frac{\bar{p}_u}{M}$ and $p_u = \frac{\bar{p}_u}{N_f}$, respectively, for $N_{tot} \in \{120, 480, 1440\}$. Fig. 6b investigates the impact of increasing the total number of antennas N_{tot} or M at the FC on the performance of the detectors for both the centralized and distributed configurations. The detection performance improves as the number of antennas deployed at the FC increases. The performance further improves upon increasing the transmit duration N . The probability of error P_e gleaned from our simulations is plotted as a function of SNR p_u in Fig. 6c for both antenna configurations along with the analytical expressions of (64) and (65). It is evident that the probability of error decreases as the SNR increases, and that the analytical results are in close agreement with the simulated P_e plots.

Fig. 8 studies the impact of increasing the density of sensors in the range of $[0.5R, R]$ on the detection performance of the proposed schemes. The trend demonstrates the performance improvement of increasing the number of sensors K . Moreover, the D-MIMO scheme outperforms the C-MIMO detector, with the performance gap widening upon increasing the sensor density. The probability of detection P_D is plotted against the path loss exponent ν in Fig. 9 for the D-MIMO detector using $N_{tot} \in \{360, 720, 1440\}$. It is evident that the detection performance degrades upon increasing the path loss exponent, which can be compensated to a certain extent by employing a larger number of antennas at the FC.

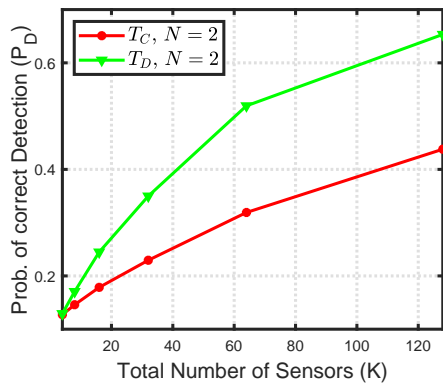


Figure 8. P_D vs. the number of sensors K for the detectors in (22) and (44) with sensors distributed in the range $[0.5R, R]$ for $N_{tot} = 1024$, $p_u = -18$ dB, $N = 2$ and $P_{FA} = 0.1$.

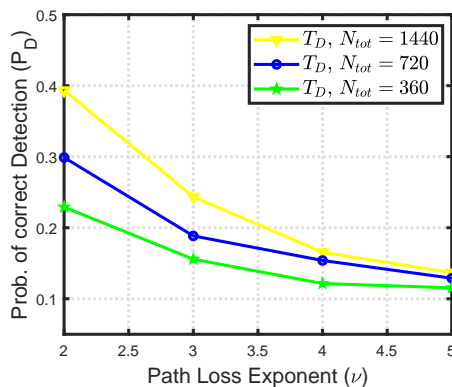


Figure 9. P_D vs. the path loss exponent ν for D-MIMO scheme with $N_{tot} \in \{360, 720, 1440\}$, $p_u = -18$ dB, $N = 2$ and $P_{FA} = 0.1$.

VIII. CONCLUSION

This paper developed distributed parameter detection schemes for a mmWave massive MIMO sensor network relying on both centralized and distributed antenna topologies, with FCS and PCS, respectively. Hybrid combining exploiting the antenna array response vectors was utilized to derive low-complexity fusion rules that also incorporate the local detection performance of the individual sensors. Furthermore, closed-form analytical expressions were obtained for the probabilities of false alarm P_{FA} and correct detection P_D . Moreover, the power scaling laws of the various detectors were determined in the large-scale antenna array regime for quantifying the sensor transmit power reduction that can be achieved as a function of the number of antennas at the FC. Additionally, the deflection coefficient maximization principle was exploited for deriving efficient transmit signaling matrices, which lead to verifiably improved detection performance. Our simulation results demonstrated that the D-MIMO WSN using the D-selection scheme outperforms the C-MIMO WSN. Based on the results obtained, it is clear that the distributed antenna architecture yields significant benefits in short-range communication and sensing in next generation WSNs. This framework can also be extended to a scenario where multiple

sensors can be assigned per FC in the distributed antenna configuration. Finally, the multi-cell scenario can also be explored, with special attention to the effects of pilot reuse.

APPENDIX A

PROOF OF THEOREM 2

The simplified test statistic $T_D(\mathbf{Z}_D)$ obtained upon substituting $\mathbf{z}_{D,k}$ from (39) into (44), can be expressed as

$$T_D(\mathbf{Z}_D) = \sum_{k=1}^K a_k d_{k,j_k} \left(\sqrt{p_u} \frac{N_f \beta_{k,j_k}}{L_{k,j_k}} |\alpha_{k,j_k}^{l_k}|^2 \mathbf{x}_k^H \mathbf{C}_{D,k}^{-1} \mathbf{u}_k + \tilde{w}_{D,R} \right),$$

where the equivalent noise $\tilde{w}_{D,R} = \Re(\tilde{\mathbf{w}}_{D,k}^H \mathbf{C}_{D,k}^{-1} \mathbf{u}_k)$ follows the Normal distribution $\tilde{w}_{D,R} \sim \mathcal{N}\left(0, \frac{\sigma_w^2 N_f d_{k,j_k} \|\mathbf{C}_{D,k}^{-1} \mathbf{u}_k\|^2}{2}\right)$. Upon using the above expression, the mean $\mu_{T_D|\mathcal{H}_1}$ under hypothesis \mathcal{H}_1 can be expressed as

$$\begin{aligned} \mu_{T_D|\mathcal{H}_1} &= \sum_{k=1}^K a_k d_{k,j_k} \left(\sqrt{p_u} N_f d_{k,j_k} \mathbb{E}\{\mathbf{x}_k^H|\mathcal{H}_1\} \mathbf{C}_{D,k}^{-1} \mathbf{u}_k \right) \\ &= \sum_{k=1}^K \sqrt{p_u} a_k b_k d_{k,j_k}^2 N_f (\mathbf{u}_k^H \mathbf{C}_{D,k}^{-1} \mathbf{u}_k). \end{aligned} \quad (66)$$

The mean $\mu_{T_D|\mathcal{H}_0}$ under hypothesis \mathcal{H}_0 and the variances $\sigma_{T_D|\mathcal{H}_1}^2, \sigma_{T_D|\mathcal{H}_0}^2$, under hypotheses \mathcal{H}_1 and \mathcal{H}_0 , respectively, can be determined along similar lines to those in Appendix A of [1].

APPENDIX B

PROOF OF THEOREM 3

The normalized mean $\mu_{T_C|\mathcal{H}_1}^a$ corresponding to the test statistic in (22) under hypothesis \mathcal{H}_1 can be expressed as

$$\mu_{T_C|\mathcal{H}_1}^a = \lim_{M \rightarrow \infty} \frac{\mu_{T_C|\mathcal{H}_1}}{\sigma_{T_C|\mathcal{H}_1}} \Bigg|_{p_u = \frac{\tilde{p}_u}{M}}. \quad (67)$$

Upon substituting the expressions of $\mu_{T_C|\mathcal{H}_1}$ and $\sigma_{T_C|\mathcal{H}_1}$, in (25) and (27), respectively, into (67), the above expression can be simplified to

$$\mu_{T_C|\mathcal{H}_1}^a = \lim_{M \rightarrow \infty} \frac{\sum_{k=1}^K \sqrt{\tilde{p}_u} a_k b_k d_k^2 \mathbf{u}_k^H (\mathbf{C}_k^a)^{-1} \mathbf{u}_k}{\sqrt{\sum_{k=1}^K d_k^2 a_k^2 \left(\tilde{p}_u \zeta_k^a + \frac{\sigma_w^2}{2} d_k \mathbf{u}_k^H (\mathbf{C}_k^a)^{-2} \mathbf{u}_k \right)}},$$

where the equivalent covariance matrix \mathbf{C}_k^a can be defined as $\mathbf{C}_k^a = \mathbf{C}_k \Big|_{p_u = \frac{\tilde{p}_u}{M}} = \frac{\tilde{p}_u \beta_k^2}{L_k^2} \mathbf{u}_k \mathbf{u}_k^H \text{var}\{|\alpha_k^{l_k}|^2\} + \sigma_w^2 d_k \mathbf{I}_N$. Similarly, the quantity ζ_k^a can be expressed as $\zeta_k^a = \zeta_k \Big|_{p_u = \frac{\tilde{p}_u}{M}} = \left(\frac{\beta_k^2}{L_k^2} \mathbb{E}\{|\alpha_k^{l_k}|^4\} - d_k^2 b_k^2 \right) (\mathbf{u}_k^H (\mathbf{C}_k^a)^{-1} \mathbf{u}_k)^2$. Following a similar procedure determines the normalized mean $\mu_{T_C|\mathcal{H}_0}^a$ under hypothesis \mathcal{H}_0 .

REFERENCES

- [1] A. Chawla, R. K. Singh, A. Patel, and A. K. Jagannatham, "Distributed detection in millimeter wave massive MIMO wireless sensor networks," in *Proceedings International Conference on Signal Processing and Communications (SPCOM)*, Jul. 2020, pp. 1–5.

- [2] R. V. Kulkarni and G. K. Venayagamoorthy, "Particle swarm optimization in wireless-sensor networks: A brief survey," *IEEE Transactions on Systems, Man, and Cybernetics, Part C (Applications and Reviews)*, vol. 41, no. 2, pp. 262–267, 2011.
- [3] I. A. Hemadeh, K. Satyanarayana, M. El-Hajjar, and L. Hanzo, "Millimeter-wave communications: Physical channel models, design considerations, antenna constructions, and link-budget," *IEEE Communications Surveys Tutorials*, vol. 20, no. 2, pp. 870–913, 2018.
- [4] T. S. Rappaport, S. Sun, and M. Shafi, "Investigation and comparison of 3GPP and NYUSIM channel models for 5G wireless communications," in *Proceedings IEEE 86th Vehicular Technology Conference (VTC-Fall)*, Sep. 2017, pp. 1–5.
- [5] D. Gesbert, M. Kountouris, R. W. Heath, C. Chae, and T. Salzer, "Shifting the MIMO paradigm," *IEEE Signal Processing Magazine*, vol. 24, no. 5, pp. 36–46, 2007.
- [6] H. Q. Ngo, E. G. Larsson, and T. L. Marzetta, "Energy and spectral efficiency of very large multiuser MIMO systems," *IEEE Transactions on Communications*, vol. 61, no. 4, pp. 1436–1449, 2013.
- [7] A. Yang, Y. Jing, C. Xing, Z. Fei, and J. Kuang, "Performance analysis and location optimization for massive MIMO systems with circularly distributed antennas," *IEEE Transactions on Wireless Communications*, vol. 14, no. 10, pp. 5659–5671, 2015.
- [8] J. Li, D. Yue, and Y. Sun, "Performance analysis of millimeter wave massive MIMO systems in centralized and distributed schemes," *IEEE Access*, vol. 6, pp. 75 482–75 494, 2018.
- [9] S. Gimenez, D. Calabuig, S. Roger, J. F. Monserrat, and N. Cardona, "Distributed hybrid precoding for indoor deployments using millimeter wave band," *Mobile Information Systems*, vol. 2017, Oct. 2017, Art. no. 5751809.
- [10] D. Yue and H. H. Nguyen, "Multiplexing gain analysis of mmWave massive MIMO systems with distributed antenna subarrays," *IEEE Transactions on Vehicular Technology*, vol. 68, no. 11, pp. 11 368–11 373, 2019.
- [11] D. Castanheira, P. Lopes, A. Silva, and A. Gameiro, "Hybrid beamforming designs for massive MIMO millimeter-wave heterogeneous systems," *IEEE Access*, vol. 5, pp. 21 806–21 817, 2017.
- [12] H. B. Almelah and K. A. Hamdi, "Spectral efficiency of distributed large-scale MIMO systems with ZF receivers," *IEEE Transactions on Vehicular Technology*, vol. 66, no. 6, pp. 4834–4844, 2017.
- [13] M. A. Al-Jarrah, A. Al-Dweik, M. Kalil, and S. S. Ikki, "Decision fusion in distributed cooperative wireless sensor networks," *IEEE Transactions on Vehicular Technology*, vol. 68, no. 1, pp. 797–811, 2019.
- [14] M. K. Banavar, A. D. Smith, C. Tepedelenlioglu, and A. Spanias, "Distributed detection over fading MACs with multiple antennas at the fusion center," in *Proceedings IEEE International Conference on Acoustics, Speech and Signal Processing (ICASSP)*, Mar. 2010, pp. 2894–2897.
- [15] D. Ciuonzo, G. Romano, and P. S. Rossi, "Channel-aware decision fusion in distributed MIMO wireless sensor networks: Decode-and-fuse vs. decode-then-fuse," *IEEE Transactions on Wireless Communications*, vol. 11, no. 8, pp. 2976–2985, 2012.
- [16] D. Ciuonzo, P. S. Rossi, and S. Dey, "Massive MIMO channel-aware decision fusion," *IEEE Transactions on Signal Processing*, vol. 63, no. 3, pp. 604–619, 2015.
- [17] A. Chawla, A. Patel, A. K. Jagannatham, and P. K. Varshney, "Distributed detection in massive MIMO wireless sensor networks under perfect and imperfect CSI," *IEEE Transactions on Signal Processing*, vol. 67, no. 15, pp. 4055–4068, 2019.
- [18] F. Sahrabi and W. Yu, "Hybrid digital and analog beamforming design for large-scale antenna arrays," *IEEE Journal of Selected Topics in Signal Processing*, vol. 10, no. 3, pp. 501–513, 2016.
- [19] O. E. Ayach, R. W. Heath, S. Abu-Surra, S. Rajagopal, and Z. Pi, "The capacity optimality of beam steering in large millimeter wave MIMO systems," in *Proceedings IEEE 13th International Workshop on Signal Processing Advances in Wireless Communications (SPAWC)*, Jun. 2012, pp. 100–104.
- [20] J. Li, L. Xiao, X. Xu, and S. Zhou, "Robust and low complexity hybrid beamforming for uplink multiuser mmWave MIMO systems," *IEEE Communications Letters*, vol. 20, no. 6, pp. 1140–1143, 2016.
- [21] Y. Chen, D. Chen, T. Jiang, and L. Hanzo, "Millimeter-wave massive MIMO systems relying on generalized sub-array-connected hybrid precoding," *IEEE Transactions on Vehicular Technology*, vol. 68, no. 9, pp. 8940–8950, 2019.
- [22] K. Satyanarayana, M. El-Hajjar, A. A. M. Mourad, and L. Hanzo, "Multi-user hybrid beamforming relying on learning-aided link-adaptation for mmWave systems," *IEEE Access*, vol. 7, pp. 23 197–23 209, 2019.
- [23] Y. Cai, Y. Xu, Q. Shi, B. Champagne, and L. Hanzo, "Robust joint hybrid transceiver design for millimeter wave full-duplex MIMO relay systems," *IEEE Transactions on Wireless Communications*, vol. 18, no. 2, pp. 1199–1215, 2019.
- [24] A. Saleh, A. J. Rustako, and R. S. Roman, "Distributed antennas for indoor radio environments," *IEEE Transactions on Communications*, vol. 35, pp. 1245–1251, 1987.
- [25] H. H. Xia, A. B. Herrera, S. Kim, and F. S. Rico, "A CDMA-distributed antenna system for in-building personal communications services," *IEEE Journal on Selected Areas in Communications*, vol. 14, no. 4, pp. 644–650, 1996.
- [26] K. J. Kerpez, "A radio access system with distributed antennas," *IEEE Transactions on Vehicular Technology*, vol. 45, no. 2, pp. 265–275, 1996.
- [27] W. Roh and A. Paulraj, "Outage performance of the distributed antenna systems in a composite fading channel," in *Proceedings IEEE 56th Vehicular Technology Conference (VTC-Fall)*, vol. 3, Sep. 2002, pp. 1520–1524.
- [28] H. Zhuang, L. Dai, L. Xiao, and Y. Yao, "Spectral efficiency of distributed antenna system with random antenna layout," *IET Electronics Letters*, vol. 39, no. 6, pp. 495–496, 2003.
- [29] L. Dai, "A comparative study on uplink sum capacity with co-located and distributed antennas," *IEEE Journal on Selected Areas in Communications*, vol. 29, no. 6, pp. 1200–1213, 2011.
- [30] E. Park, S. Lee, and I. Lee, "Antenna placement optimization for distributed antenna systems," *IEEE Transactions on Wireless Communications*, vol. 11, no. 7, pp. 2468–2477, 2012.
- [31] S. Yang and L. Hanzo, "Fifty years of MIMO detection: The road to large-scale MIMOs," *IEEE Communications Surveys Tutorials*, vol. 17, no. 4, pp. 1941–1988, 2015.
- [32] O. E. Ayach, S. Rajagopal, S. Abu-Surra, Z. Pi, and R. W. Heath, "Spatially sparse precoding in millimeter wave MIMO systems," *IEEE Transactions on Wireless Communications*, vol. 13, no. 3, pp. 1499–1513, 2014.
- [33] D. Zhang, Y. Wang, X. Li, and W. Xiang, "Hybridly connected structure for hybrid beamforming in mmWave massive MIMO systems," *IEEE Transactions on Communications*, vol. 66, no. 2, pp. 662–674, 2018.
- [34] J. A. Zhang, X. Huang, V. Dyadyuk, and Y. J. Guo, "Massive hybrid antenna array for millimeter-wave cellular communications," *IEEE Transactions on Wireless Communications*, vol. 22, no. 1, pp. 79–87, 2015.
- [35] K. Satyanarayana, M. El-Hajjar, P. Kuo, A. Mourad, and L. Hanzo, "Dual-function hybrid beamforming and transmit diversity aided millimeter wave architecture," *IEEE Transactions on Vehicular Technology*, vol. 67, no. 3, pp. 2798–2803, 2018.
- [36] W. Li and H. Dai, "Distributed detection in wireless sensor networks using a multiple access channel," *IEEE Transactions on Signal Processing*, vol. 55, no. 3, pp. 822–833, 2007.
- [37] A. Chawla, A. Patel, A. K. Jagannatham, and P. K. Varshney, "Robust distributed detection in massive MIMO wireless sensor networks under CSI uncertainty," in *Proceedings IEEE 88th Vehicular Technology Conference (VTC-Fall)*, Aug. 2018, pp. 1–5.
- [38] A. Chawla, A. S. Sarode, A. K. Jagannatham, and L. Hanzo, "Distributed parameter detection in massive MIMO wireless sensor networks relying on imperfect CSI," *IEEE Transactions on Wireless Communications*, vol. 20, no. 1, pp. 506–519, 2021.
- [39] F. Jiang, J. Chen, A. L. Swindlehurst, and J. A. López-Salcedo, "Massive MIMO for wireless sensing with a coherent multiple access channel," *IEEE Transactions on Signal Processing*, vol. 63, no. 12, pp. 3005–3017, 2015.
- [40] IEEE 5G Technical Community. 2017., *IEEE 5G and beyond technology roadmap white paper*. Technical Report. IEEE.
- [41] R. Niu, B. Chen, and P. K. Varshney, "Fusion of decisions transmitted over Rayleigh fading channels in wireless sensor networks," *IEEE Transactions on Signal Processing*, vol. 54, no. 3, pp. 1018–1027, 2006.
- [42] J. Chamberland and V. V. Veeravalli, "Wireless sensors in distributed detection applications," *IEEE Signal Processing Magazine*, vol. 24, no. 3, pp. 16–25, 2007.
- [43] B. Chen, L. Tong, and P. K. Varshney, "Channel-aware distributed detection in wireless sensor networks," *IEEE Signal Processing Magazine*, vol. 23, no. 4, pp. 16–26, 2006.
- [44] P. Salvo Rossi, D. Ciuonzo, K. Kansanen, and T. Ekman, "Performance analysis of energy detection for MIMO decision fusion in wireless sensor networks over arbitrary fading channels," *IEEE Transactions on Wireless Communications*, vol. 15, no. 11, pp. 7794–7806, 2016.
- [45] M. K. Banavar, A. D. Smith, C. Tepedelenlioglu, and A. Spanias, "On the effectiveness of multiple antennas in distributed detection over fading

- MACs,” *IEEE Transactions on Wireless Communications*, vol. 11, no. 5, pp. 1744–1752, 2012.
- [46] F. Jiang, J. Chen, and A. L. Swindlehurst, “Estimation in phase-shift and forward wireless sensor networks,” *IEEE Transactions on Signal Processing*, vol. 61, no. 15, pp. 3840–3851, 2013.
- [47] B. Chen, R. Jiang, T. Kasetkasem, and P. K. Varshney, “Channel aware decision fusion in wireless sensor networks,” *IEEE Transactions on Signal Processing*, vol. 52, no. 12, pp. 3454–3458, 2004.
- [48] A. A. M. Saleh and R. Valenzuela, “A statistical model for indoor multipath propagation,” *IEEE Journal on Selected Areas in Communications*, vol. 5, no. 2, pp. 128–137, 1987.
- [49] S. M. Kay, *Fundamentals of statistical signal processing, volume 2: Detection theory*. New Jersey: Prentice-Hall Inc, 1993.
- [50] S. Zhou, W. Xu, H. Zhang, and X. You, “Hybrid precoding for millimeter wave massive MIMO with analog combining,” in *Proceedings 9th International Conference on Wireless Communications and Signal Processing (WCSP)*, Oct. 2017, pp. 1–5.
- [51] A. Chawla, R. K. Singh, A. Patel, A. K. Jagannatham, and L. Hanzo, “TR.DD.2021.1: Distributed detection for centralized and decentralized millimeter wave massive MIMO sensor networks,” IIT Kanpur, Tech. Rep., 2020, [Online]. Available: http://www.iitk.ac.in/mwn/documents/TR_DDP_MMIMO_2021.pdf.
- [52] J. Li, D. Yue, and Y. Sun, “Performance analysis of millimeter wave massive MIMO systems in centralized and distributed schemes,” *IEEE Access*, vol. 6, pp. 75 482–75 494, 2018.
- [53] S. Boyd and L. Vandenberghe, *Convex optimization*. New York, NY, USA: Cambridge University Press, 2004.